Recent developments of the Material Point Method for the simulation of landslides

Eduardo Alonso, Alba Yerro, Núria Pinyol

Department of Geotechnical Engineering and Geosciences

Civil Engineering School, UPC, Barcelona

University of Warwick, September 11-15 , 2015

Outline of presentation

1. Theoretical framework
2. First failures in brittle materials
3. Deep seated fast landslides
4. Rainfall-induced landslides

Three-Phase MPM discretization

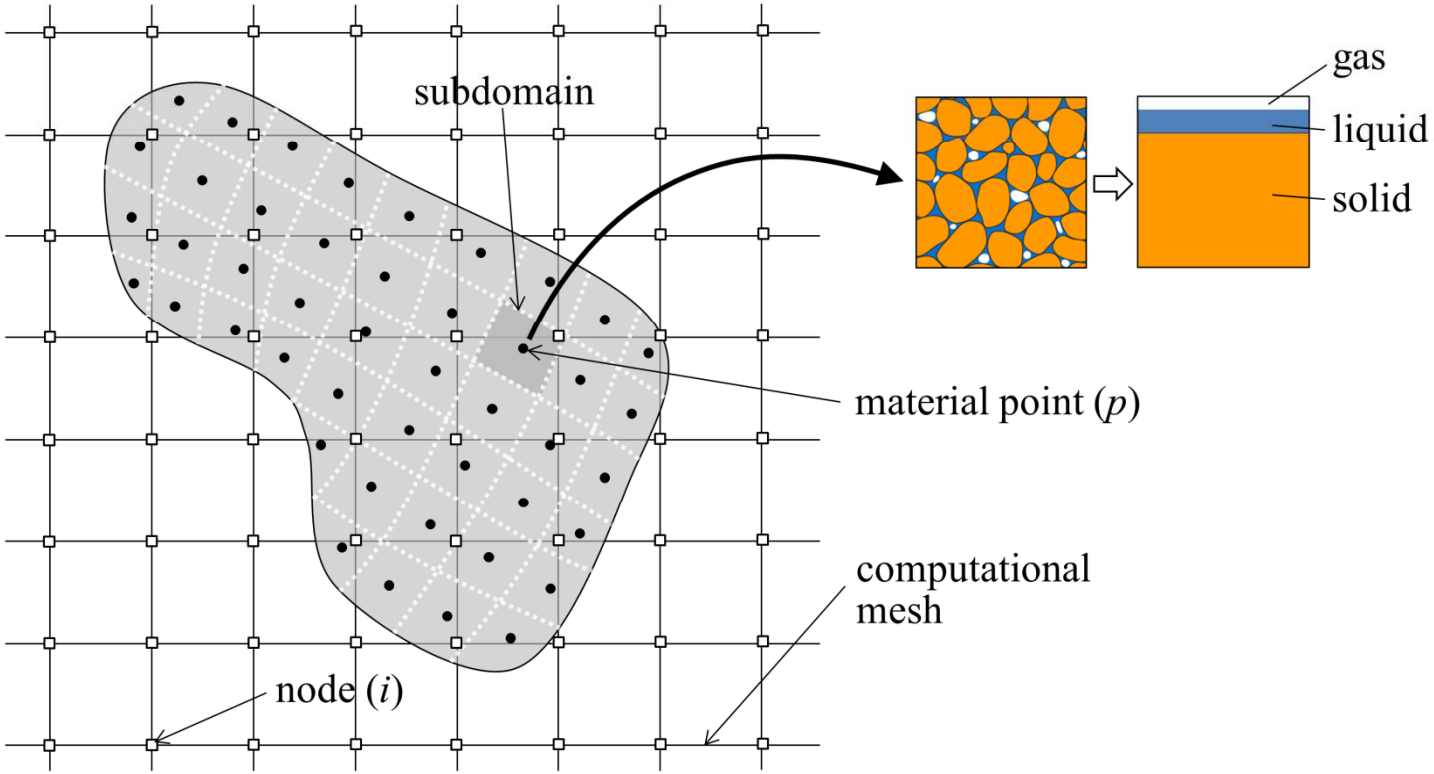

Governing equations

1) Dynamic equilibrium Liquid

$$\rho_l \dot{\mathbf{v}}_l = \nabla p_l - \frac{nS_l \mu_l}{k_l}\left(\mathbf{v}_l - \mathbf{v}_s\right) + \rho_l \mathbf{b}$$

2) Dynamic equilibrium Gas

$$\rho_g \dot{\mathbf{v}}_g = \nabla p_g - \frac{nS_g \mu_g}{k_g}\left(\mathbf{v}_g - \mathbf{v}_s\right) + \rho_g \mathbf{b}$$

3) Dynamic equilibrium Mixture

$$\rho_s \left(1-n\right)\dot{\mathbf{v}}_s + \rho_l nS_l \dot{\mathbf{v}}_l + \rho_g nS_g \dot{\mathbf{v}}_g = \nabla \cdot \boldsymbol{\sigma} + \rho_m \mathbf{b}$$

In the **nodes**

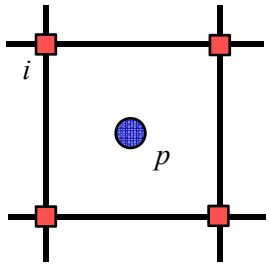

4) Mass balance Solid

$$\frac{\partial}{\partial t}\left((1-n)\rho_s\right) + \nabla \cdot \left((1-n)\rho_s \mathbf{v}_s\right) = 0$$

5) Mass balance Water

$$\frac{\partial}{\partial t}\left(\omega_g^w \rho_g S_g n + \omega_l^w \rho_l S_l n\right) + \nabla \cdot \left(\mathbf{j}_g^w + \mathbf{j}_l^w\right) = 0$$

6) Mass balance Air

$$\frac{\partial}{\partial t}\left(\omega_g^a \rho_g S_g n + \omega_l^a \rho_l S_l n\right) + \nabla \cdot \left(\mathbf{j}_g^a + \mathbf{j}_l^a\right) = 0$$

7) Constitutive equations

In the **material points**

Computational cycle

i — *explicit scheme in time*

Initialization at a *mp* level

Nodal mass matrices, *nodal* forces, *nodal* velocities

Nodal non-advective fluxes $\mathbf{i}_l^a, \mathbf{i}_g^w$

Dynamic Equilibrium Liquid

$$\tilde{\mathbf{M}}_l \cdot \dot{\mathbf{v}}_l = \mathbf{F}_l^{ext} - \mathbf{F}_l^{int} - \mathbf{Q}_l \cdot (\mathbf{v}_l - \mathbf{v}_s)$$

Dynamic Equilibrium Gas

$$\tilde{\mathbf{M}}_g \cdot \dot{\mathbf{v}}_g = \mathbf{F}_g^{ext} - \mathbf{F}_g^{int} - \mathbf{Q}_g \cdot (\mathbf{v}_g - \mathbf{v}_s)$$

Dynamic Equilibrium Mixture

$$\mathbf{M}_s \cdot \dot{\mathbf{v}}_s + \mathbf{M}_l \cdot \dot{\mathbf{v}}_l + \mathbf{M}_g \cdot \dot{\mathbf{v}}_g = \mathbf{F}^{ext} - \mathbf{F}^{int}$$

Updating *nodal* velocities

Updating *mp* velocities

Updating *mp* strains

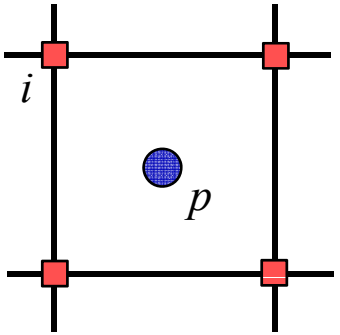

Mass balance water

$$n\frac{\partial \xi^w}{\partial p_l}\dot{p}_l + n\frac{\partial \xi^w}{\partial p_g}\dot{p}_g = -\nabla\cdot\left[n\xi_g^w(\mathbf{v}_g - \mathbf{v}_s)\right] - \nabla\cdot\left[n\xi_l^w(\mathbf{v}_l - \mathbf{v}_s)\right] - \xi^w\nabla\cdot\mathbf{v}_s - \nabla\cdot\mathbf{i}_g^w$$

Mass balance air

$$n\frac{\partial \xi^a}{\partial p_l}\dot{p}_l + n\frac{\partial \xi^a}{\partial p_g}\dot{p}_g = -\nabla\cdot\left[n\xi_g^a(\mathbf{v}_g - \mathbf{v}_s)\right] - \nabla\cdot\left[n\xi_l^a(\mathbf{v}_l - \mathbf{v}_s)\right] - \xi^a\nabla\cdot\mathbf{v}_s - \nabla\cdot\mathbf{i}_l^a$$

Constitutive equation

$$\dot{\boldsymbol{\sigma}}' = \mathbf{D} : \dot{\boldsymbol{\varepsilon}} + \mathbf{h}'\dot{s}$$

Hydraulic constitutive equations

Updating stresses and other *mp* properties

p

Material properties

- Porosity $\frac{Dn}{Dt} = \frac{(1-n)}{\rho_s}\frac{D\rho_s}{Dt} + (1-n)\nabla\cdot\mathbf{v}_s$ ($\frac{D\rho_s}{Dt} \approx 0$) (Mass balance of the solid)
- Liquid phase density $\rho_l = \rho_{l_0}\exp\left[\beta\left(p_l - p_{l_o}\right)\right]$
- Degree Saturation $S_l\left(p_l, p_g\right)$ (Retention curve)
- Liquid hydraulic conductivity $k_l(p_l, p_g)$ (Hillel expression)
- Gas phase density $\rho_g\left(p_l, p_g\right)$ (Ideal gases law)
- Mass fraction of air in liquid $\omega_l^a\left(p_g\right)$ (Henry's law)
- Mass fraction of water in gas $\omega_g^w\left(p_l, p_g\right)$ (Psychrometric law)

- Others: Bishop's parameter, viscosities..

Strain Softening Mohr-Coulomb

Yield function

$$q = c'\cos\varphi' + p'\sin\varphi'$$

Softening rules

$$\begin{cases} c' = c'_r + \left(c'_p - c'_r\right) e^{-\eta \varepsilon^p_{eq}} \\ \varphi' = \varphi_r' + \left(\varphi_p' - \varphi_r'\right) e^{-\eta \varepsilon^p_{eq}} \end{cases}$$

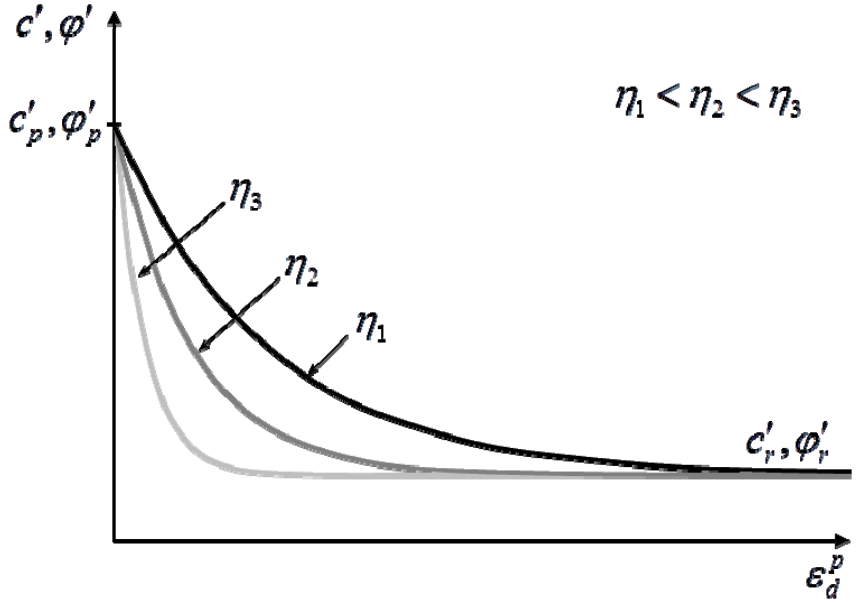

c'_r, c'_p residual and peak effective cohesion

φ'_r, φ'_p residual and peak effective friction angle

ε^p_{eq} deviatoric plastic strain

η shape factor parameter

Suction-dependent Mohr-Coulomb model

Yield function

$$q = c\cos\varphi + \bar{p}\sin\varphi$$

Softening rules (wetting softening)

$$\begin{cases} c = c' + \Delta c_{max}\left(1 - e^{-B(s/p_{atm})}\right) \\ \varphi = \varphi' + A\dfrac{s}{p_{atm}} \end{cases}$$

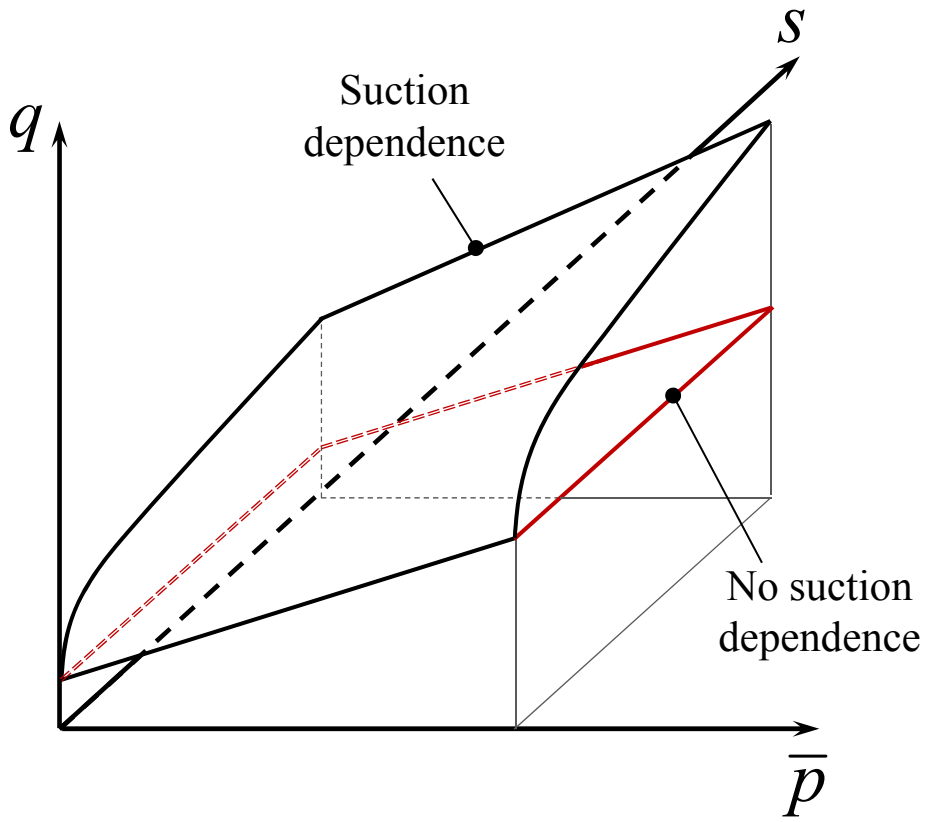

s suction

$\bar{\sigma}$ net stress

c, φ cohesion, friction angle

c', φ' cohesion, friction angle (sat cond.)

p_{atm} atmospheric pressure

$A, B, \Delta c_{max}$ model parameters

The Selborne failure experiment

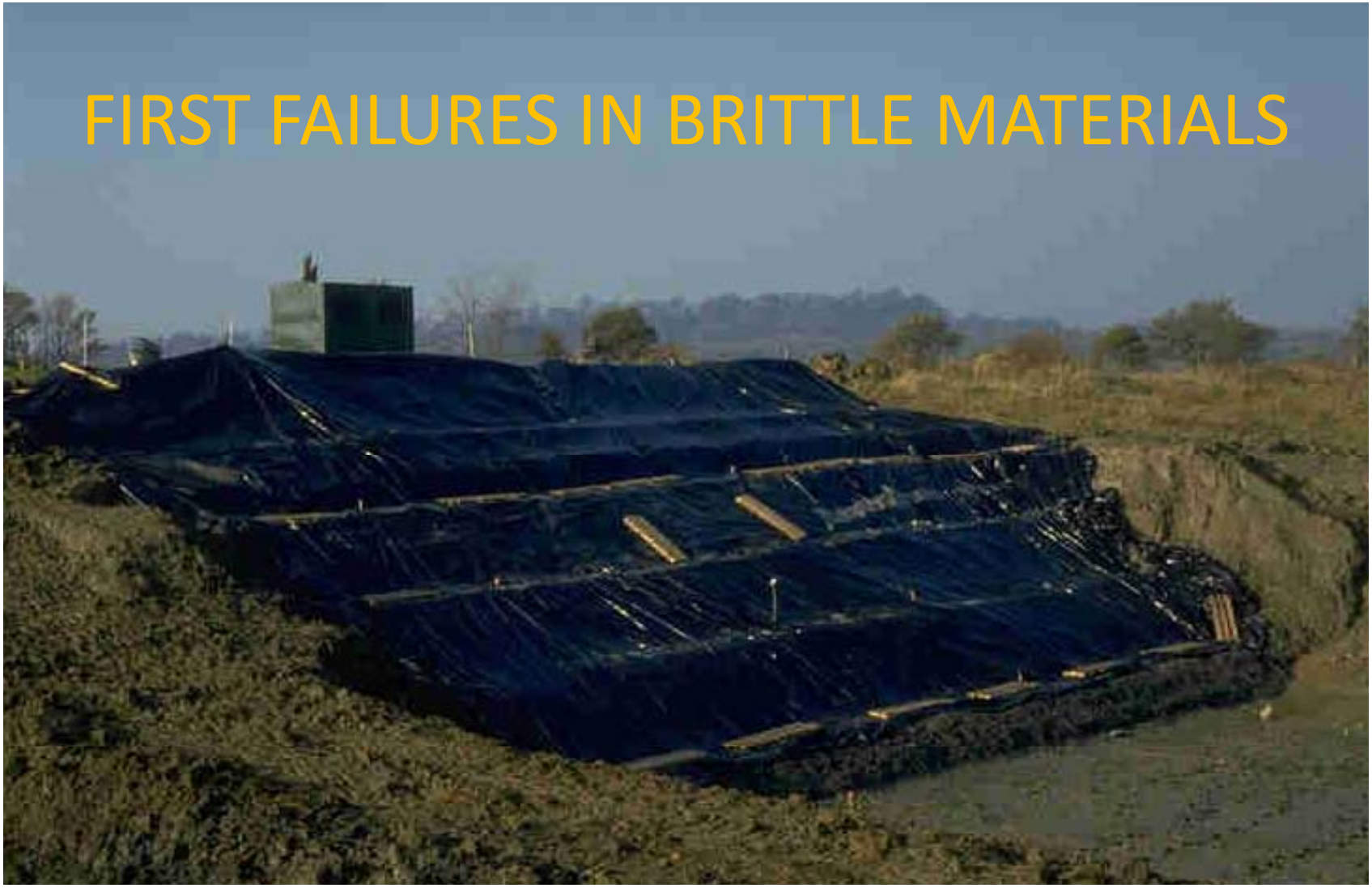

Grant, D. (1996)

The Selborne failure experiment

Grant, D. (1996)

Geometry and material parameters

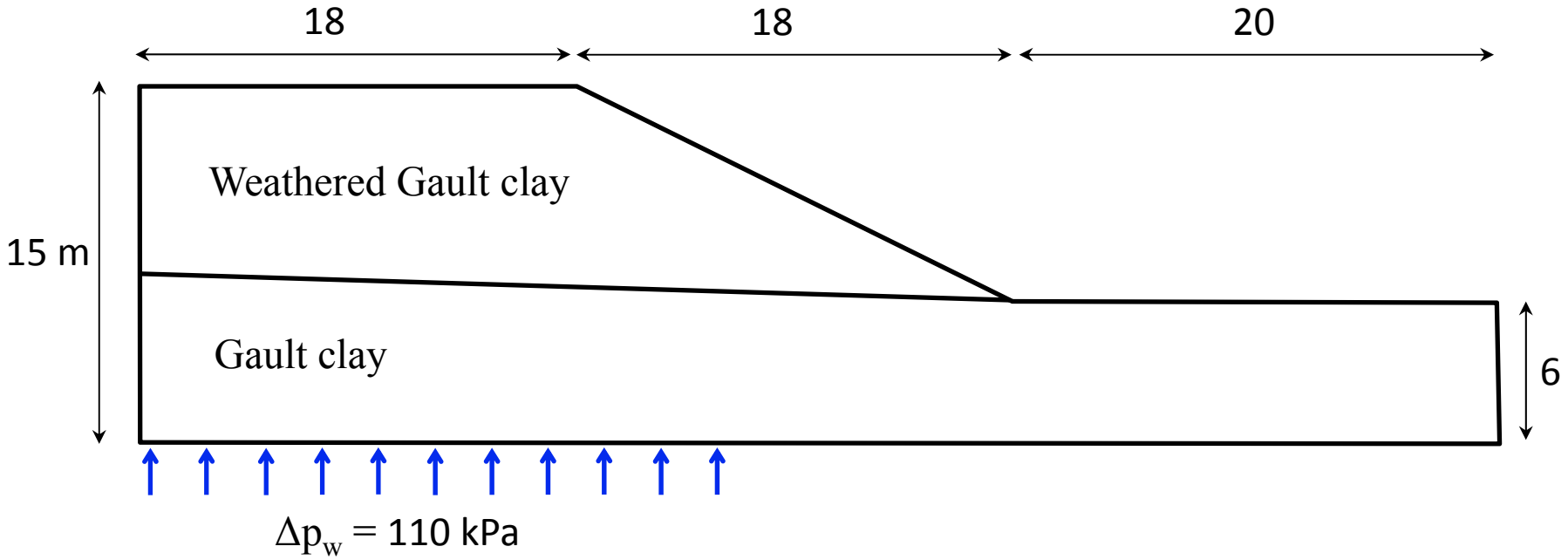

Weathered Gault clay	
Porosity	0.2
Permeability (m/s)	0.001
Dry unit weight (kN/m^3)	2500
Young modulus (kPa)	20000
Poisson's coefficient	0.33
EffectiveCohesion (peak/residual) (kPa)	**13 / 4,7**
Friction angle (peak/residual) (º)	**24,5 / 13,5**
Calibration parameter, η	500

Gault clay	
Porosity	0.2
Permeability (m/s)	0.001
Dry unit weight (kN/m^3)	2500
Young modulus (kPa)	20000
Poisson's coefficient	0.33
Cohesion (peak/residual) (kPa)	**25 / 1**
Friction angle (peak/residual) (º)	**26 / 15**
Calibration parameter, η	500

Cooper, M., Bromhead, E., Petley, D., & Grant, D. (1998)

MPM discretization

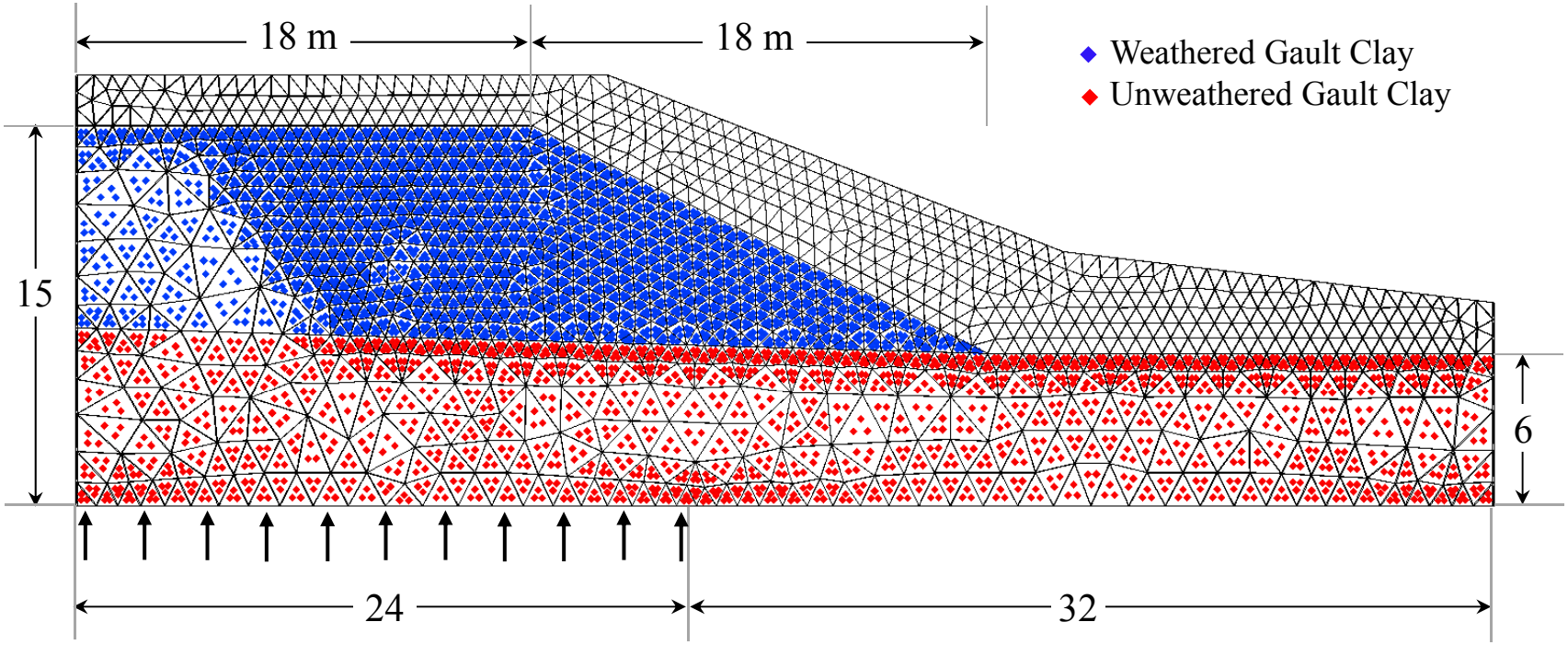

Water recharge

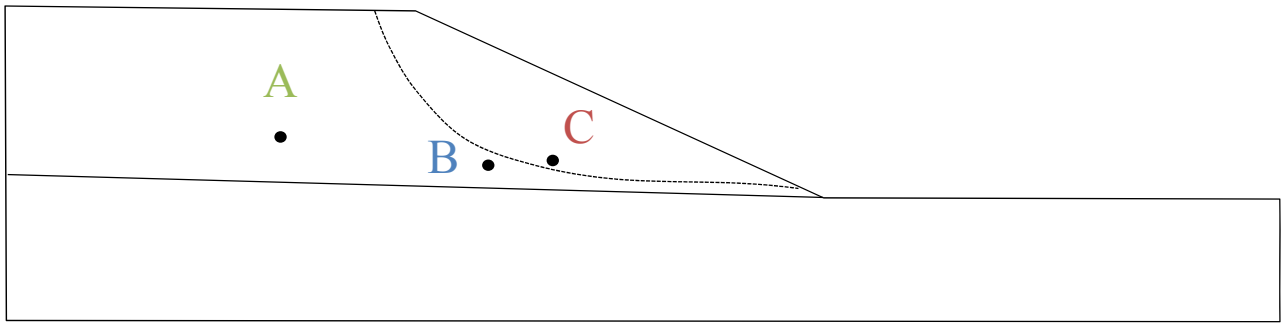

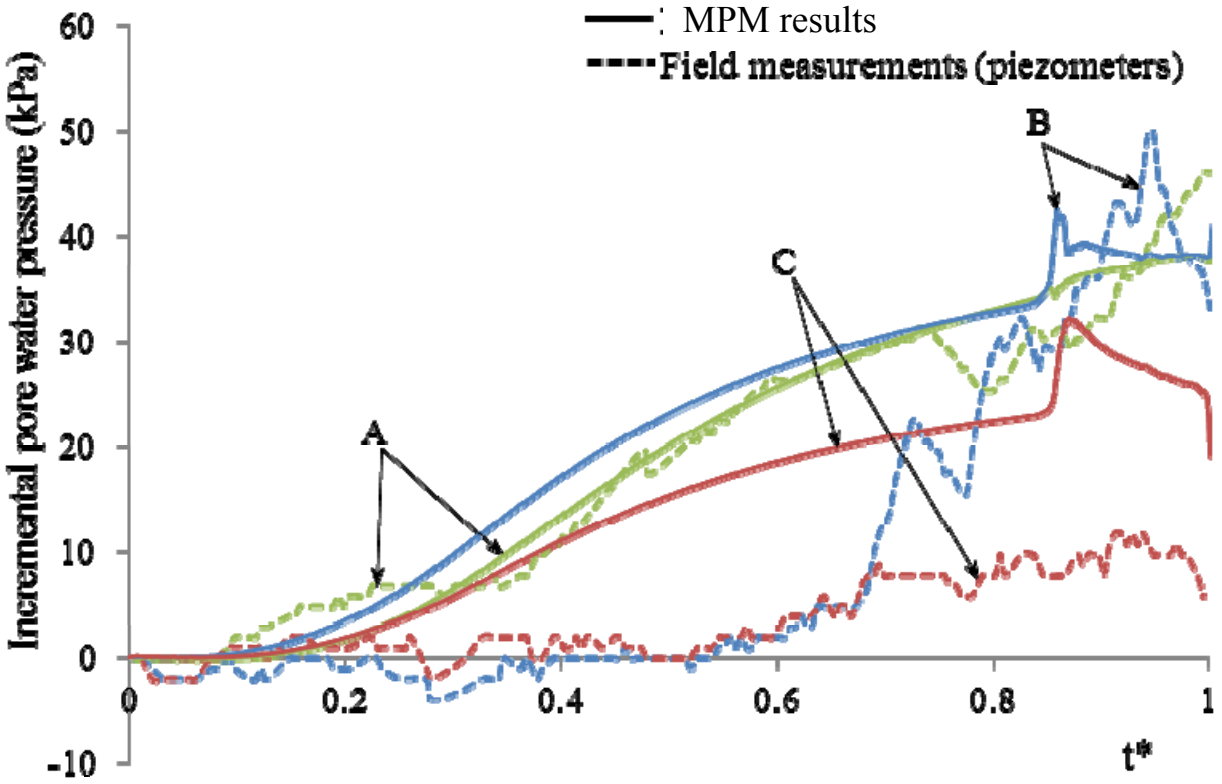

t* = time /time to failure

Initial failure mechanism

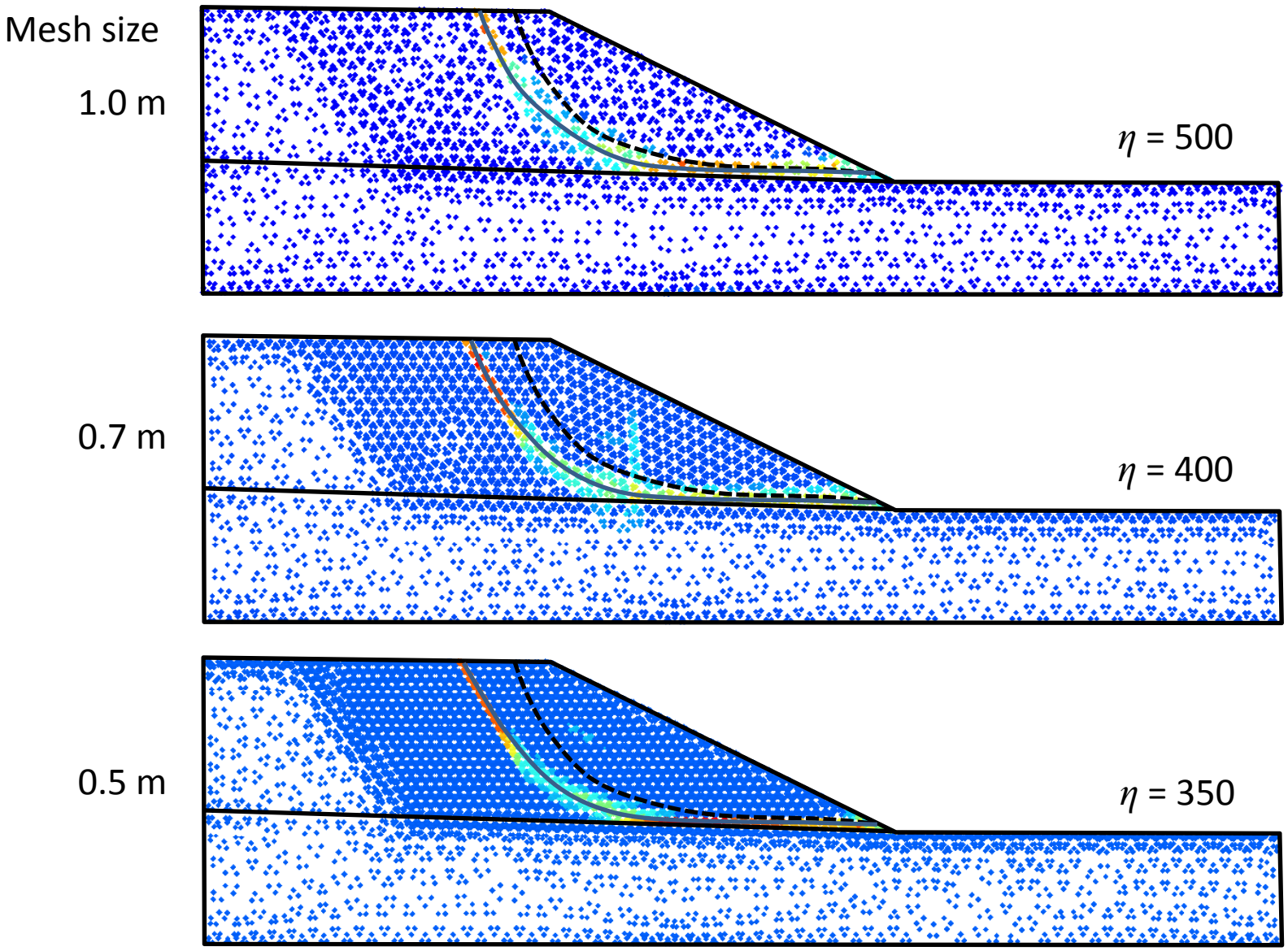

Surface movements

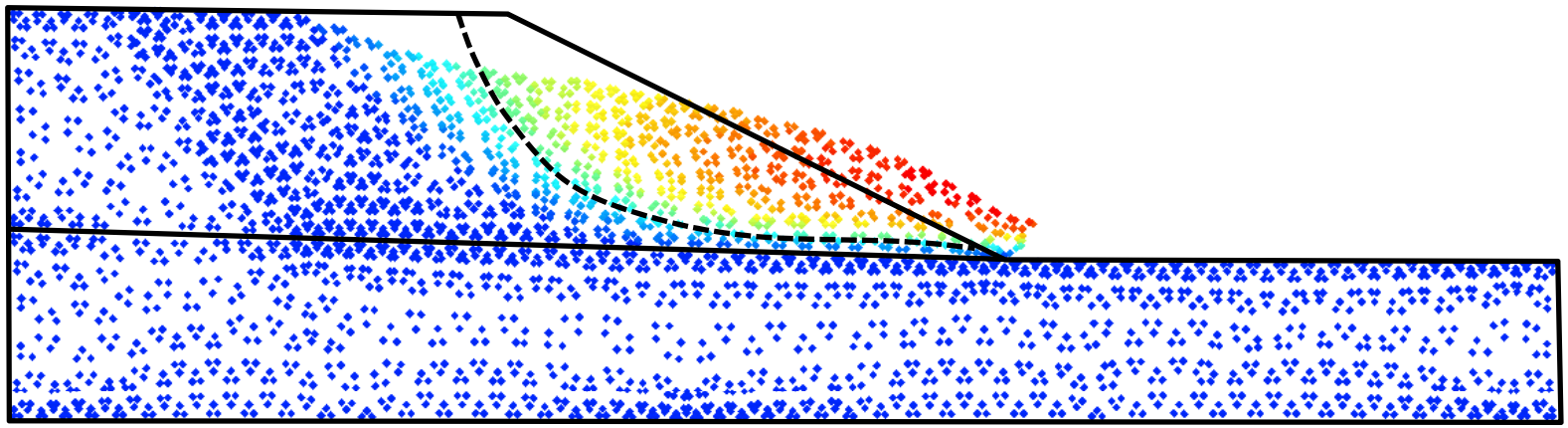

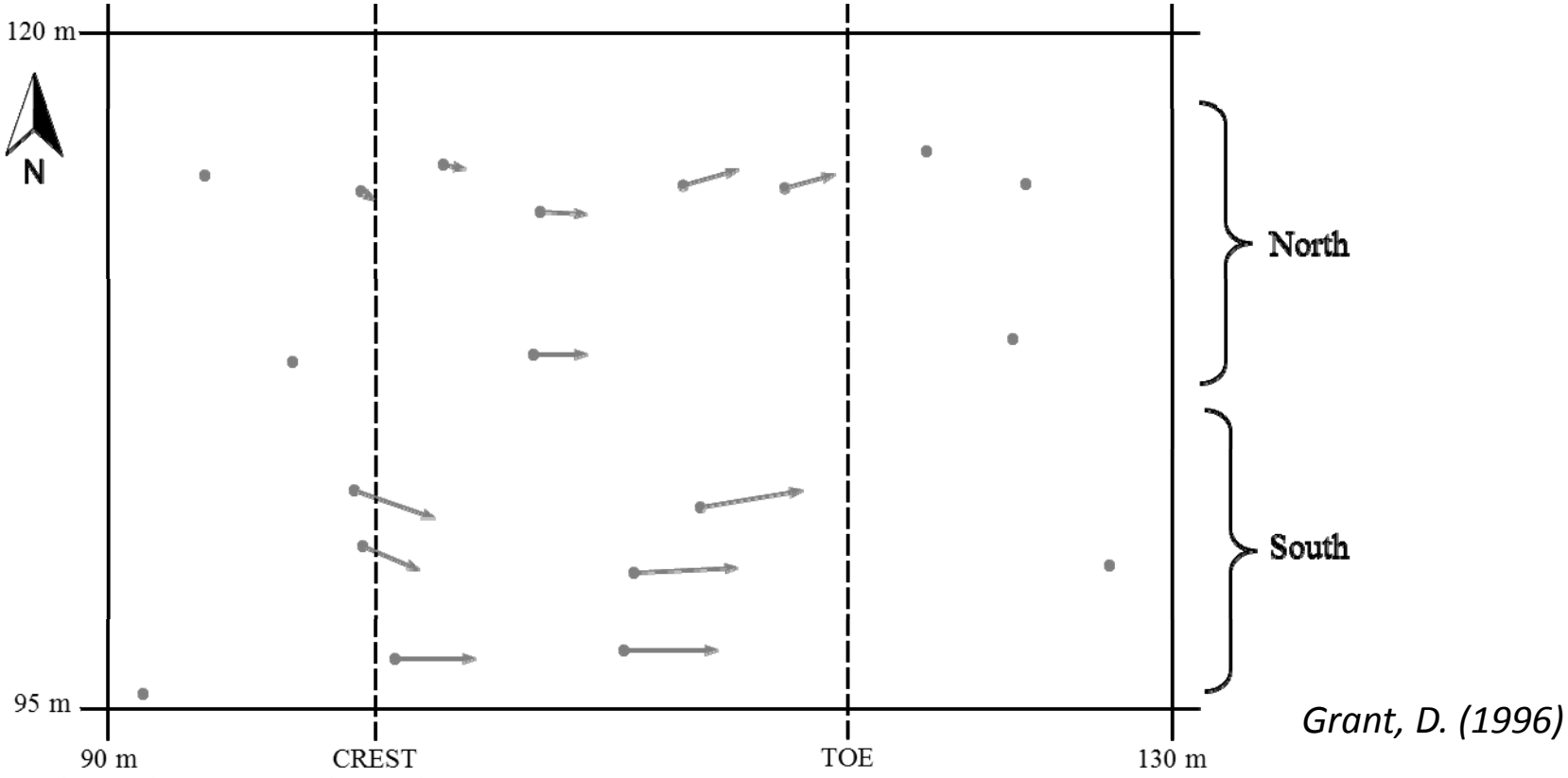

Grant, D. (1996)

Surface movements

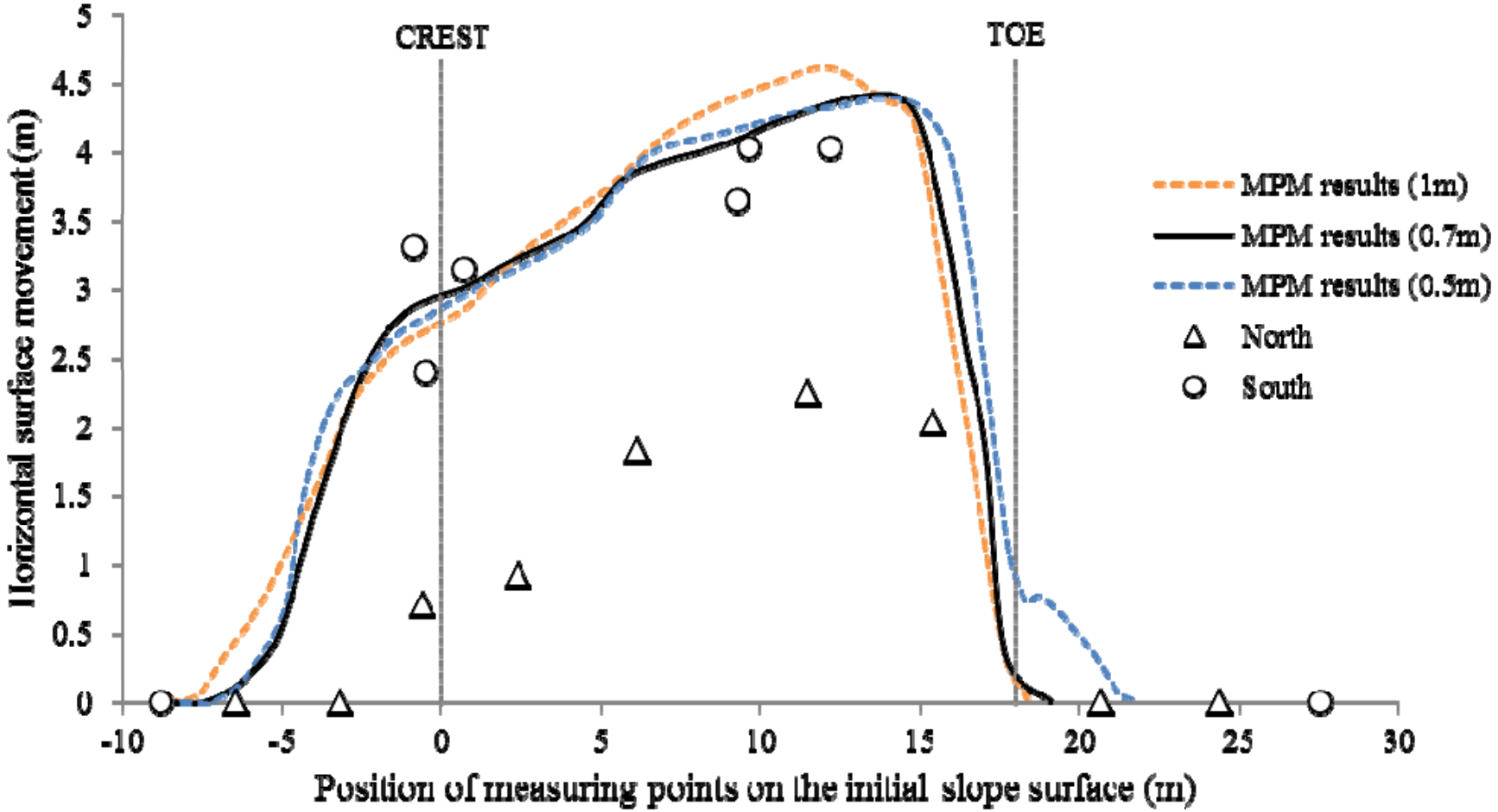

Inclinometers

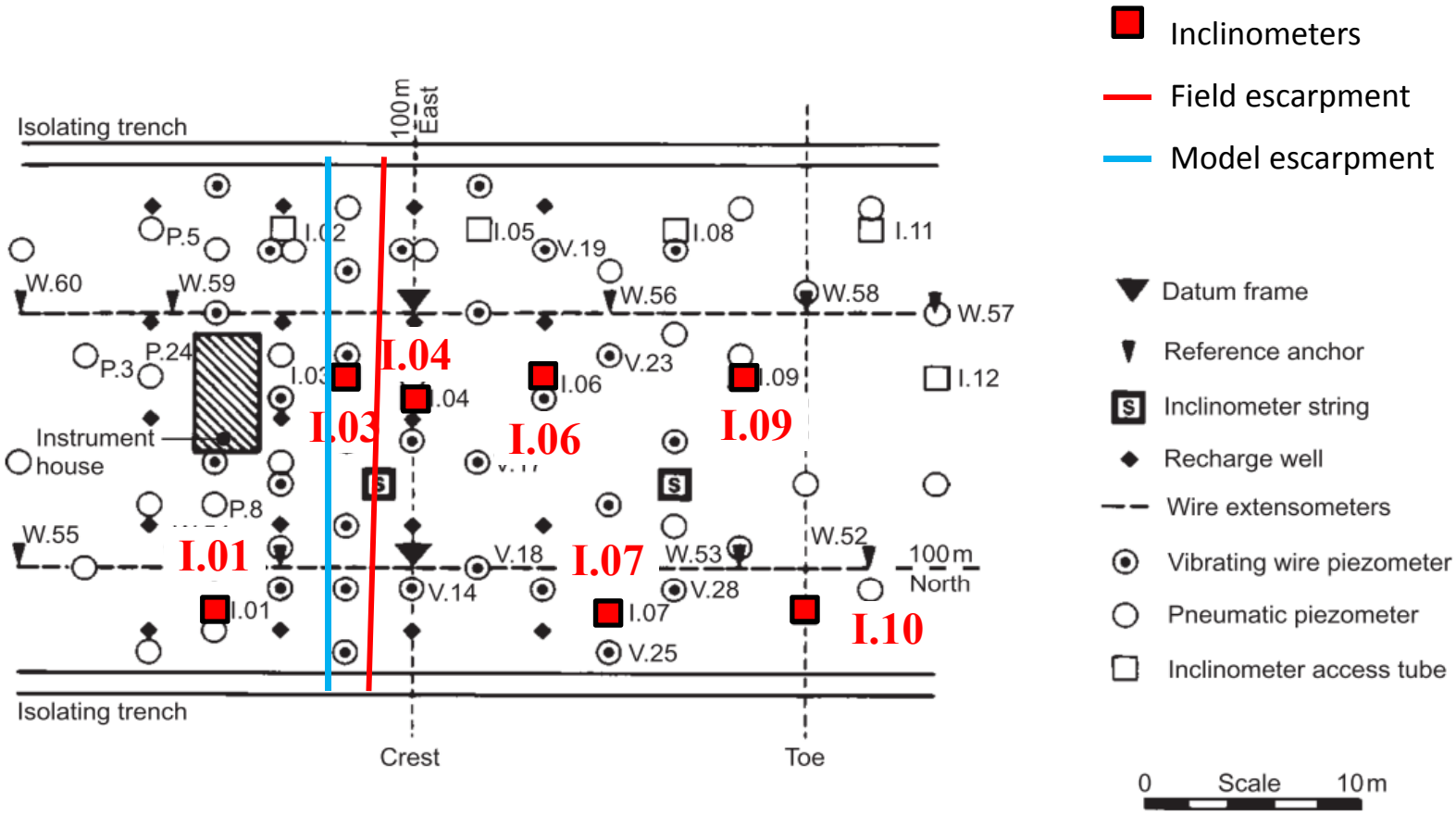

Fig. 5. Instrumentation layout plan

Cooper, M., Bromhead, E., Petley, D., & Grant, D. (1998)

Inclinometers

I.06

Displacement measured in the inclinometer I.06 between 27-January-89 and 29-June-89 (corresponds to t^*=0.93)

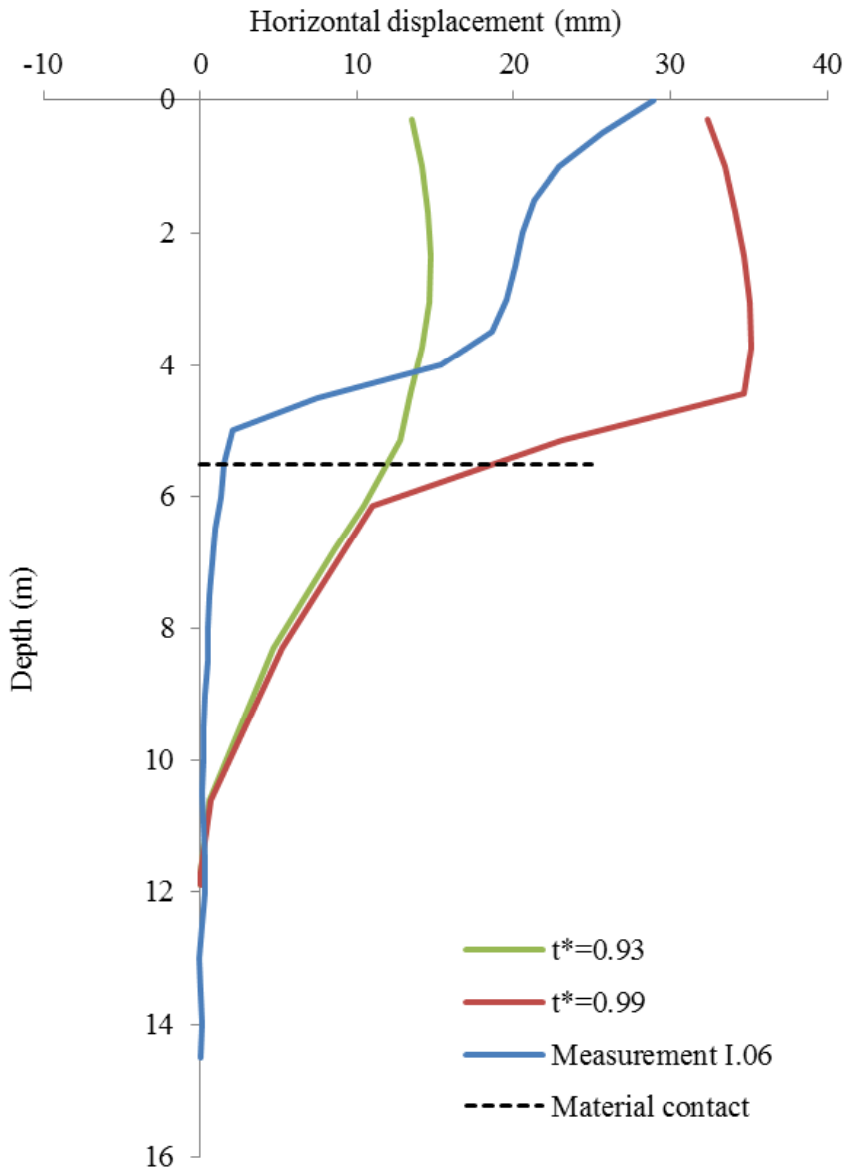

Inclinometers

I.09

Displacement measured in the inclinometer I.0 between 27-January-89 and 29-June-89 (corresponds to t^*=0.93)

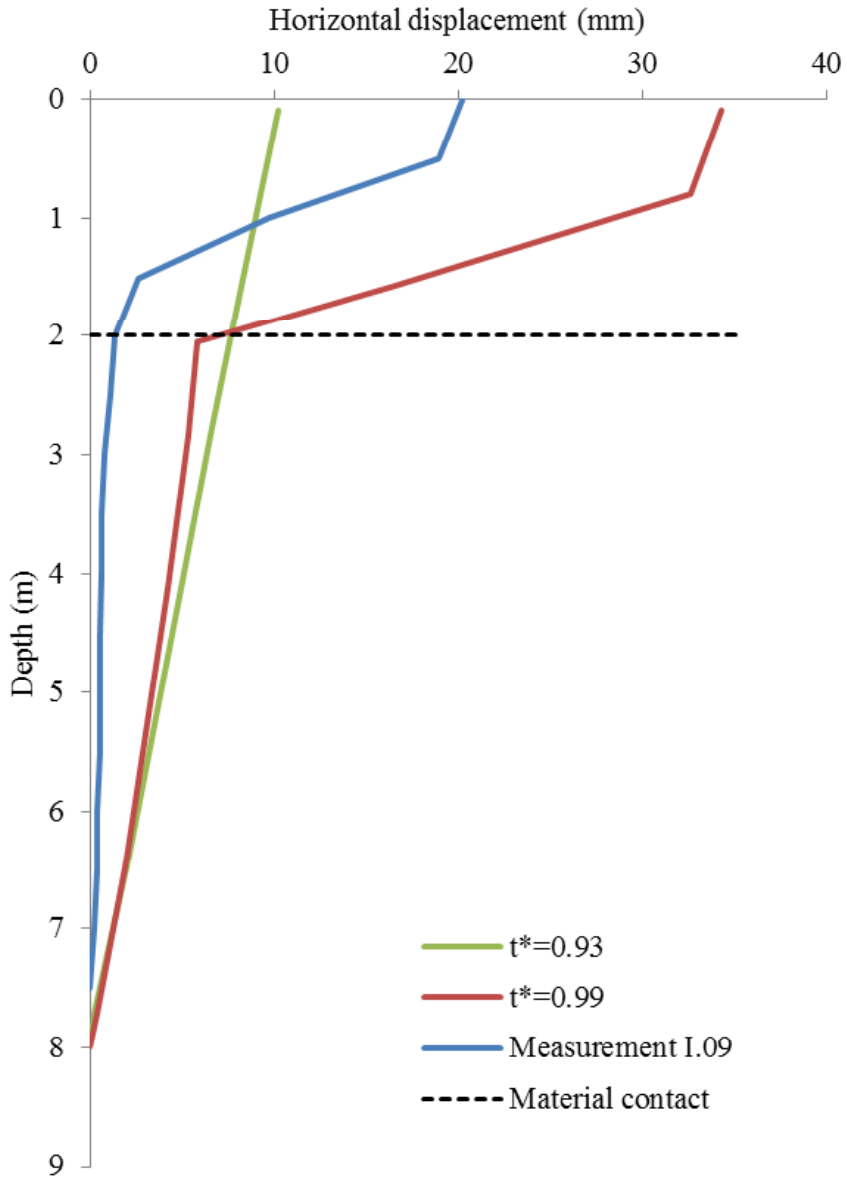

Progressive failure. Elastic behaviour

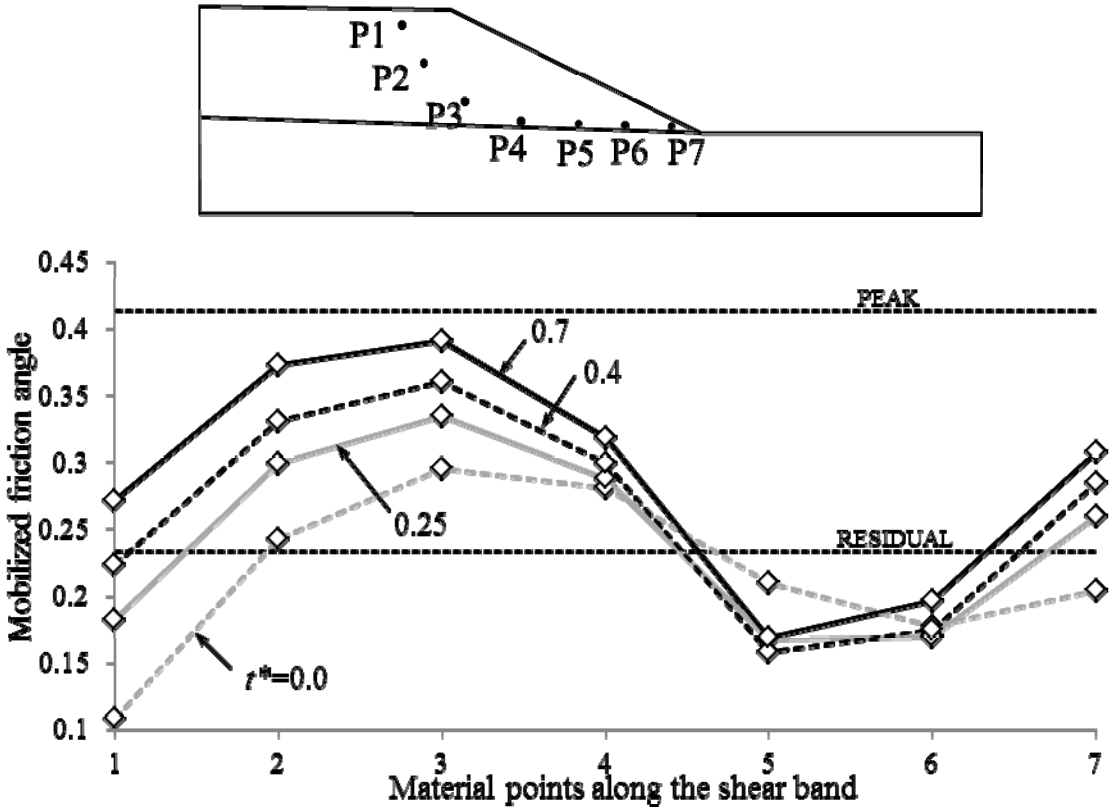

Mobilized friction angle

$$MFA = \frac{q}{p' + c' \text{cotan} \varphi'}$$

Progressive failure. Plastification starts

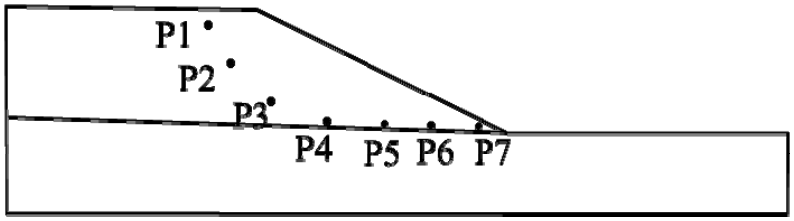

Mobilized friction angle

$$MFA = \frac{q}{p' + c' \text{cotan} \varphi'}$$

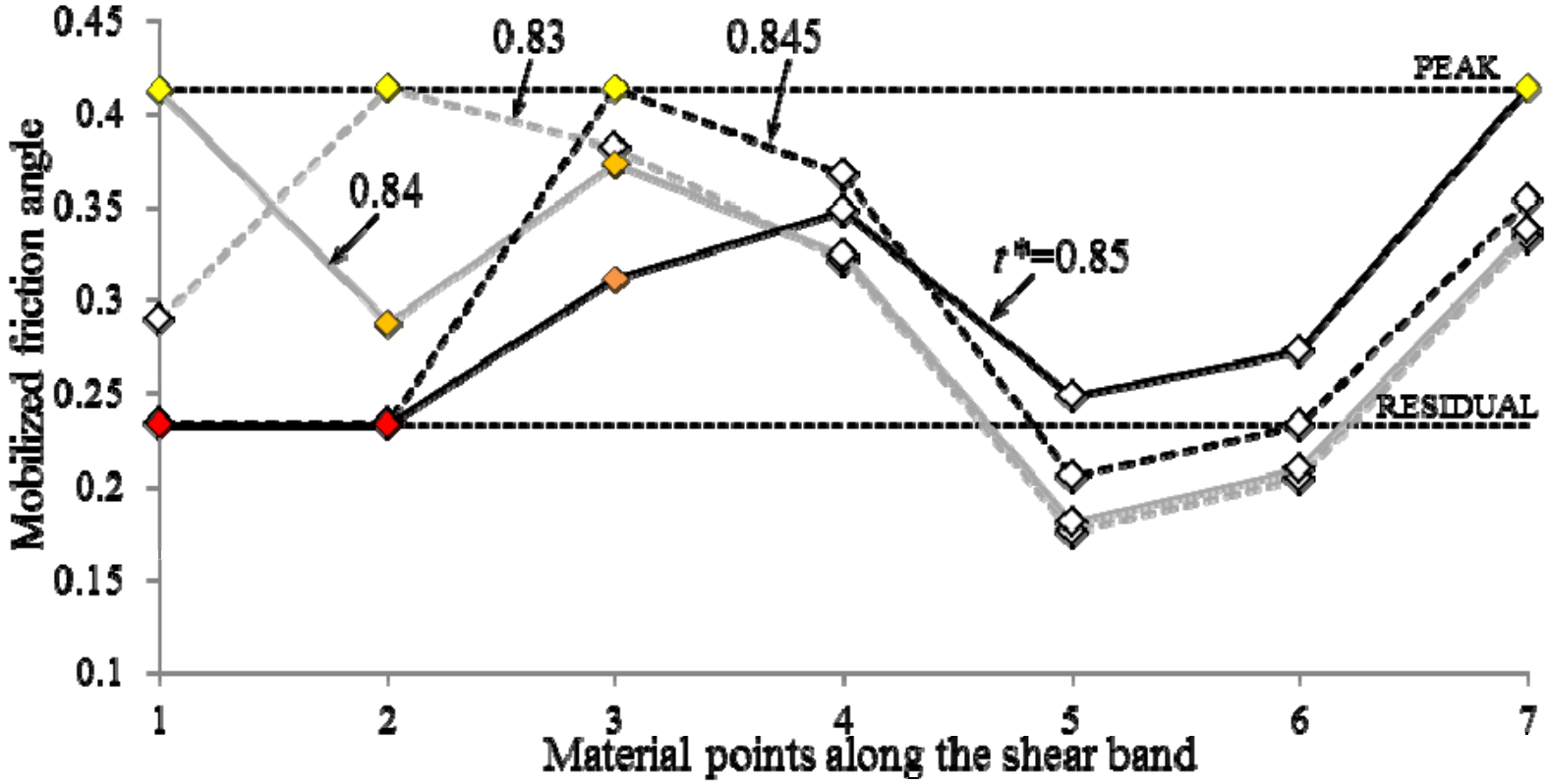

Progressive failure. Final stages

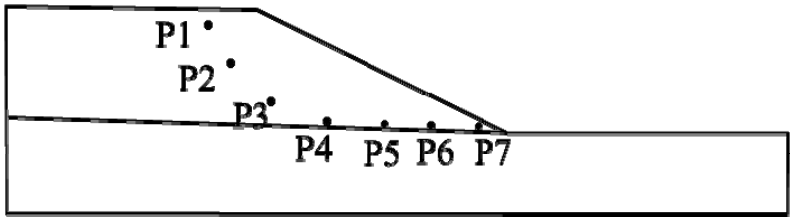

Mobilized friction angle

$$MFA = \frac{q}{p' + c' \text{cotan} \varphi'}$$

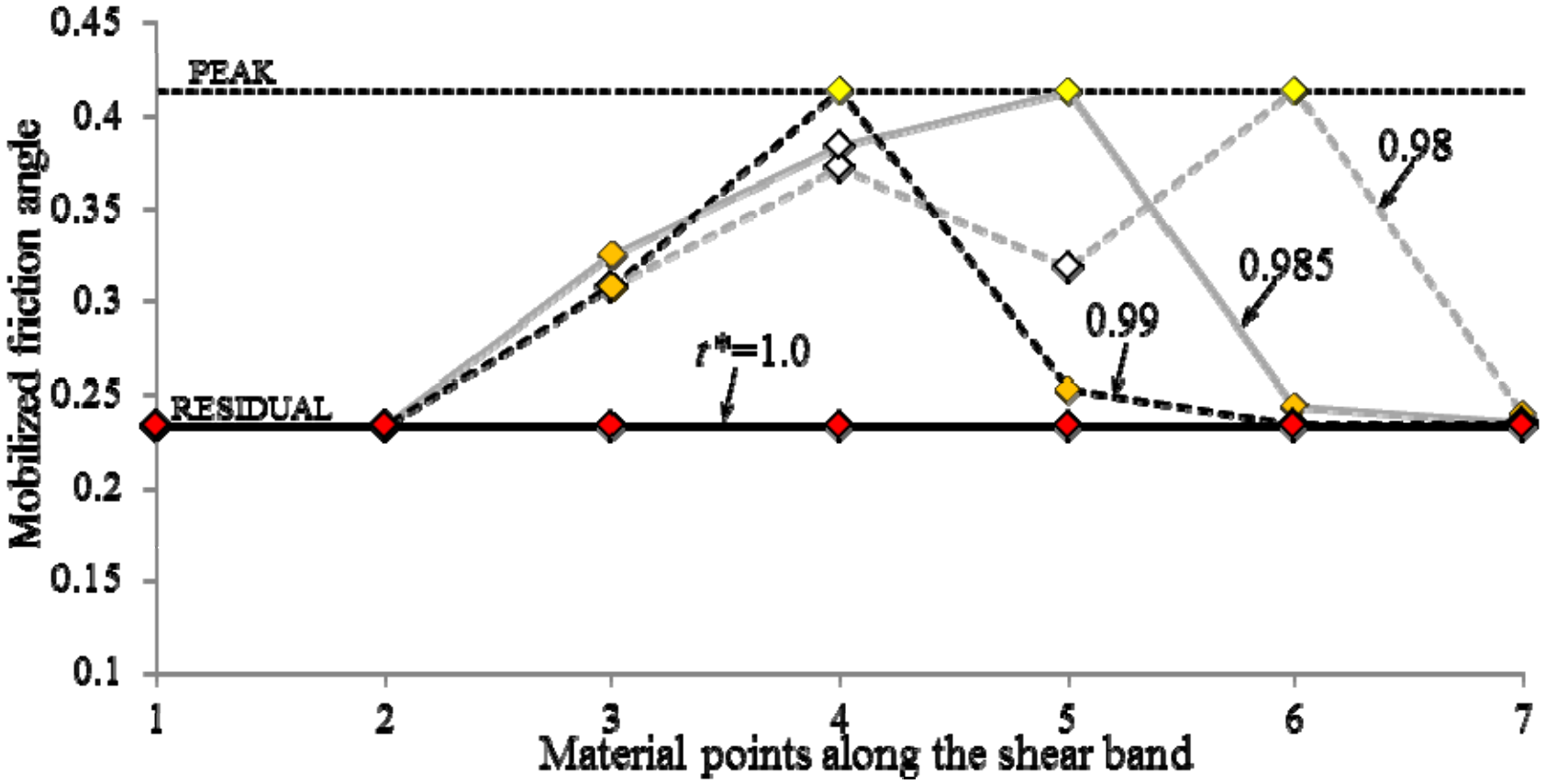

Progressive failure. Mean Mobilized Friction Angle

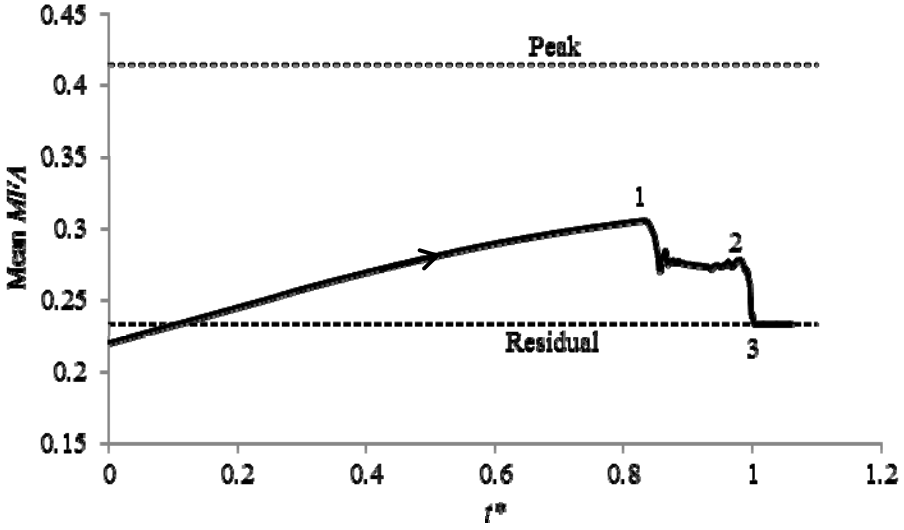

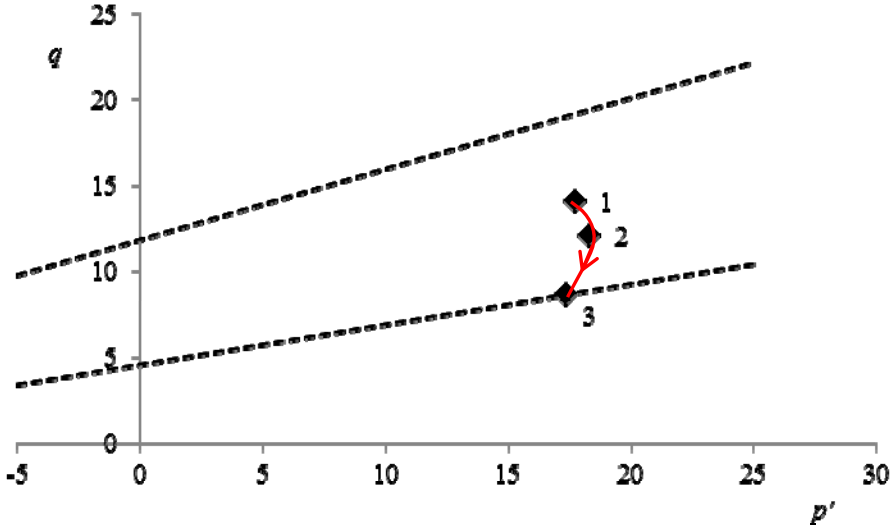

Taking 33 material points along the initial failure mechanism

t* = time /time to failure

Kinematics

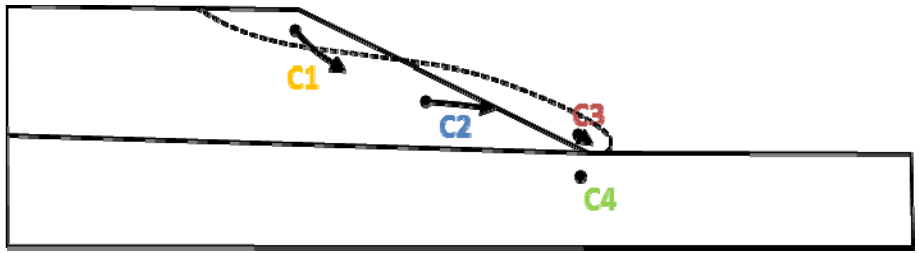
C1
C2
C3
C4

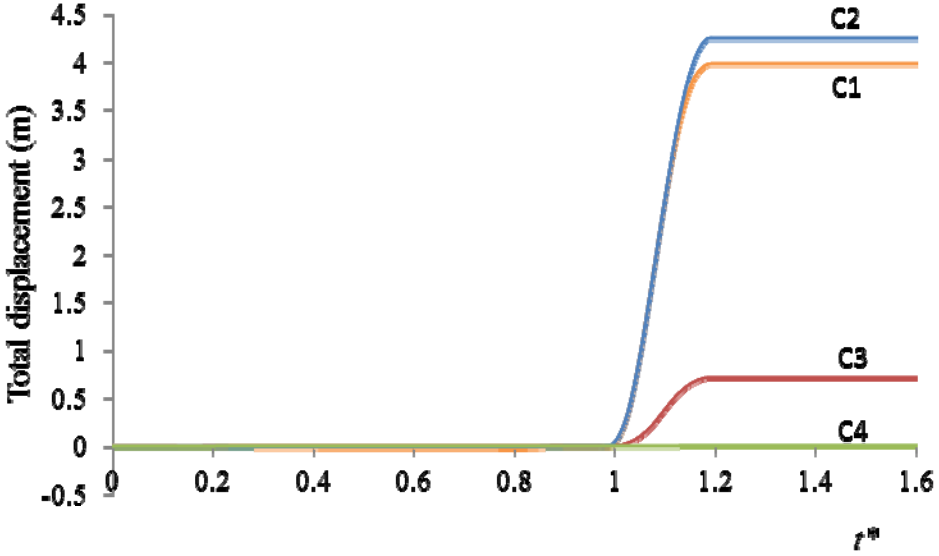
Total displacement (m)
4.5
4
3.5
3
2.5
2
1.5
1
0.5
0
-0.5
0
0.2
0.4
0.6
0.8
1
1.2
1.4
1.6
C2
C1
C3
C4

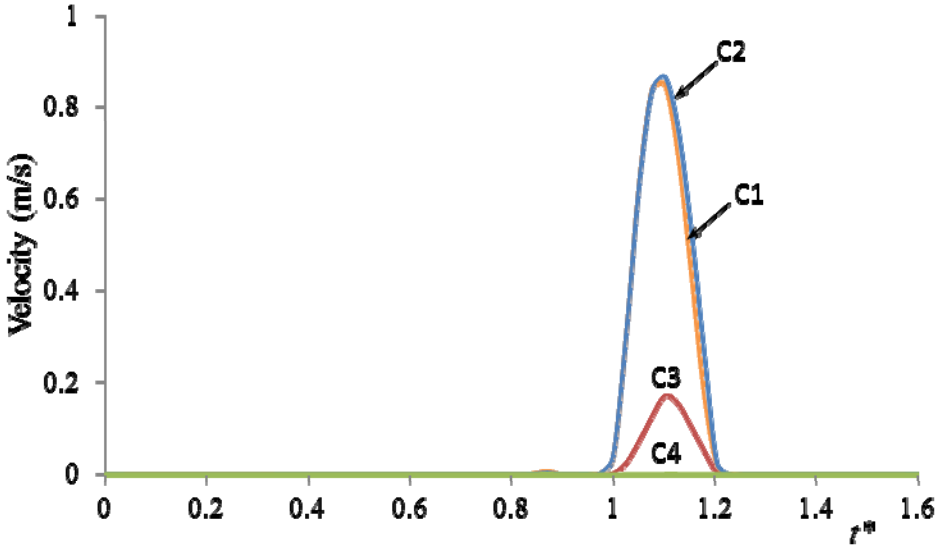
Velocity (m/s)
1
0.8
0.6
0.4
0.2
0
0
0.2
0.4
0.6
0.8
1
1.2
1.4
1.6
C2
C1
C3
C4

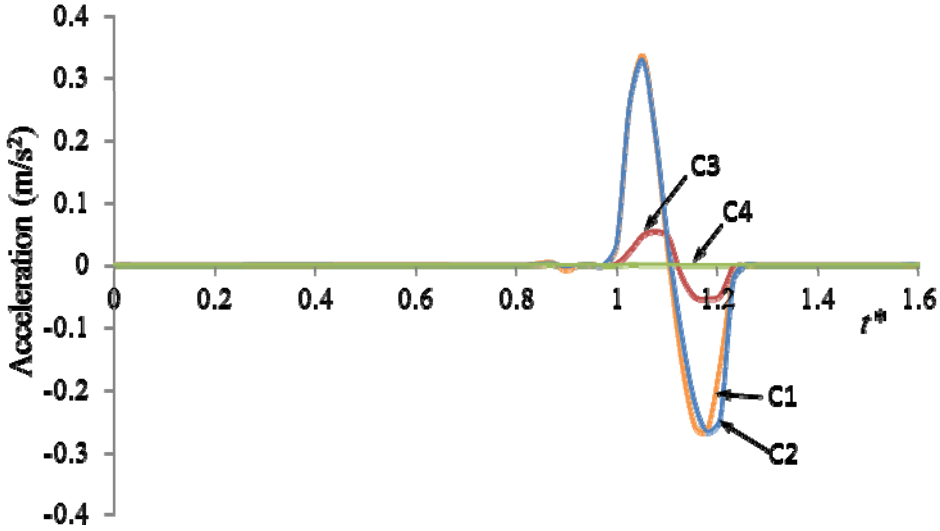
Acceleration (m/s²)
0.4
0.3
0.2
0.1
0
-0.1
-0.2
-0.3
-0.4
0
0.2
0.4
0.6
0.8
1
1.2
1.4
1.6
C3
C4
C1
C2

Stress path *p'*-*q*

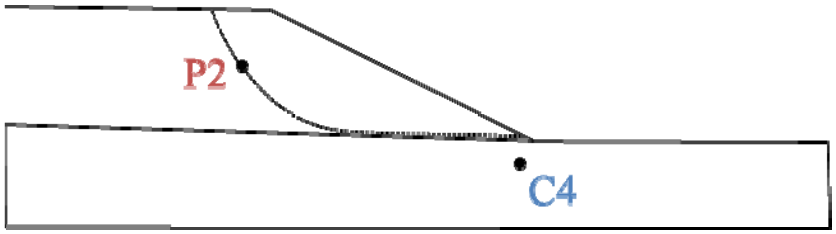

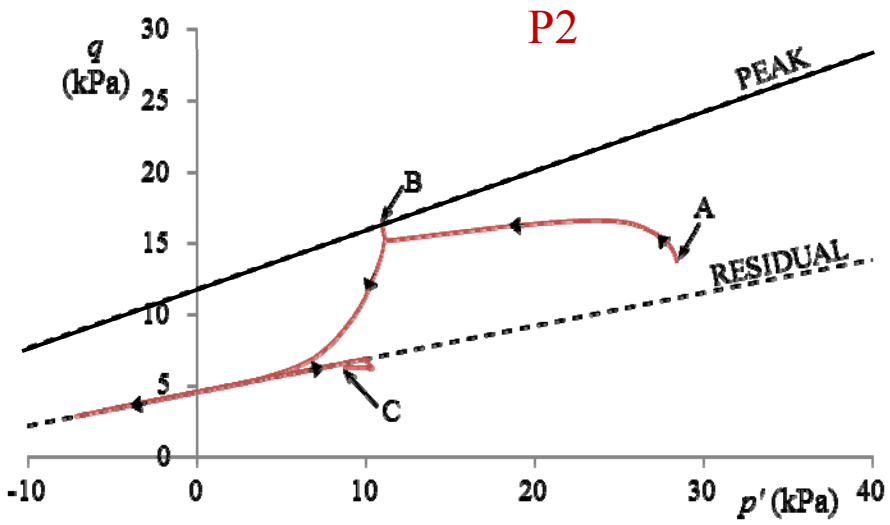

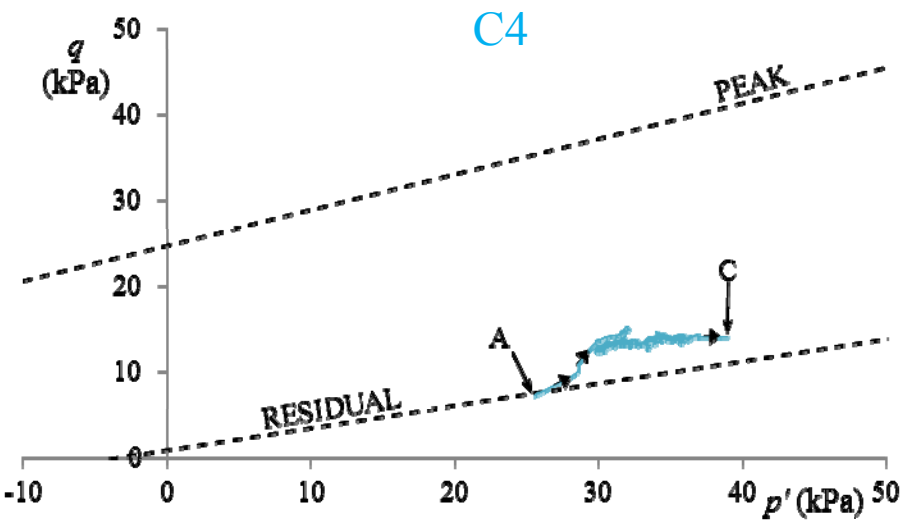

Overall instability process

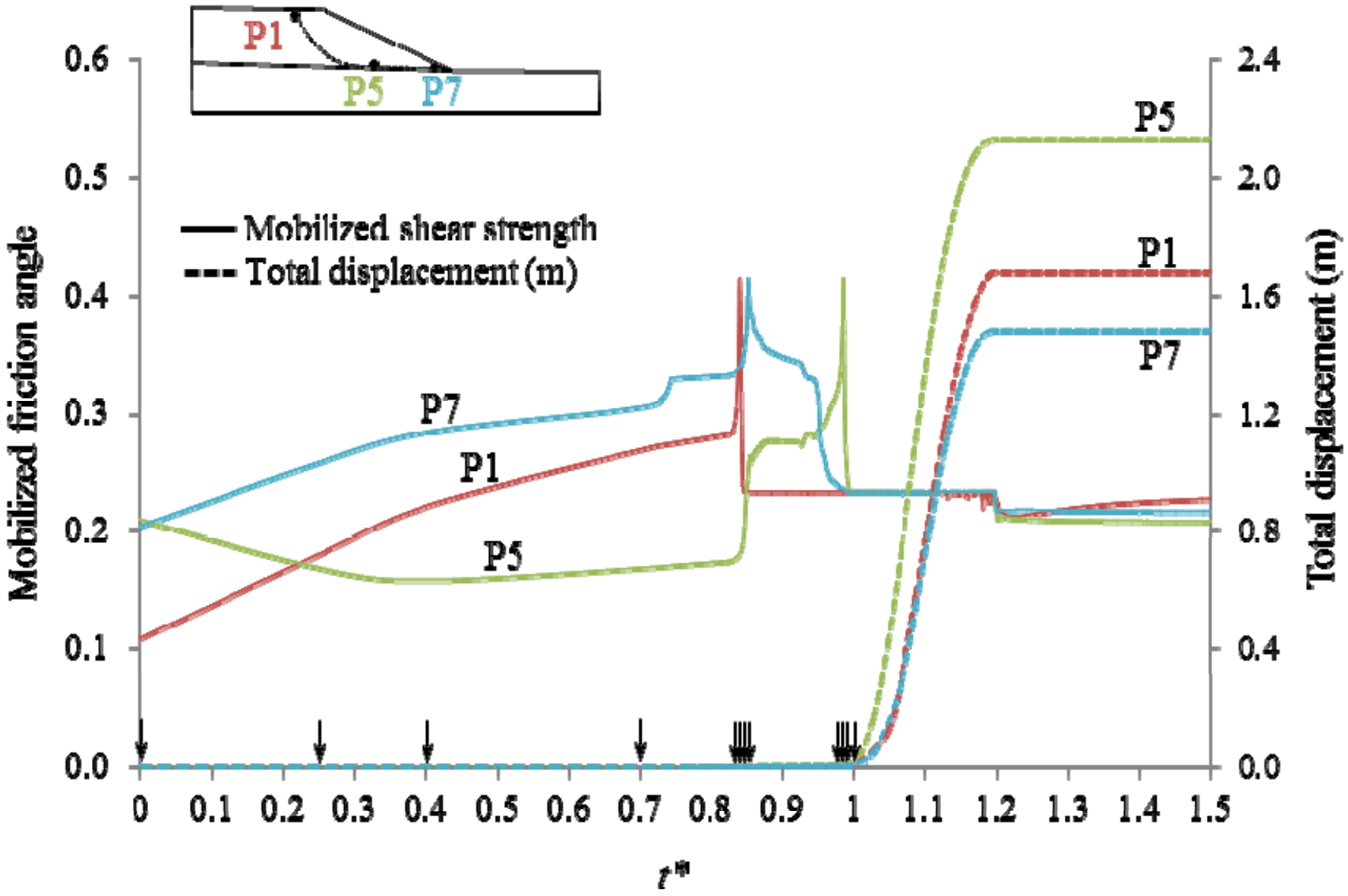


DEEP SEATED FAST LANDSLIDES
Ward & Day, 2011

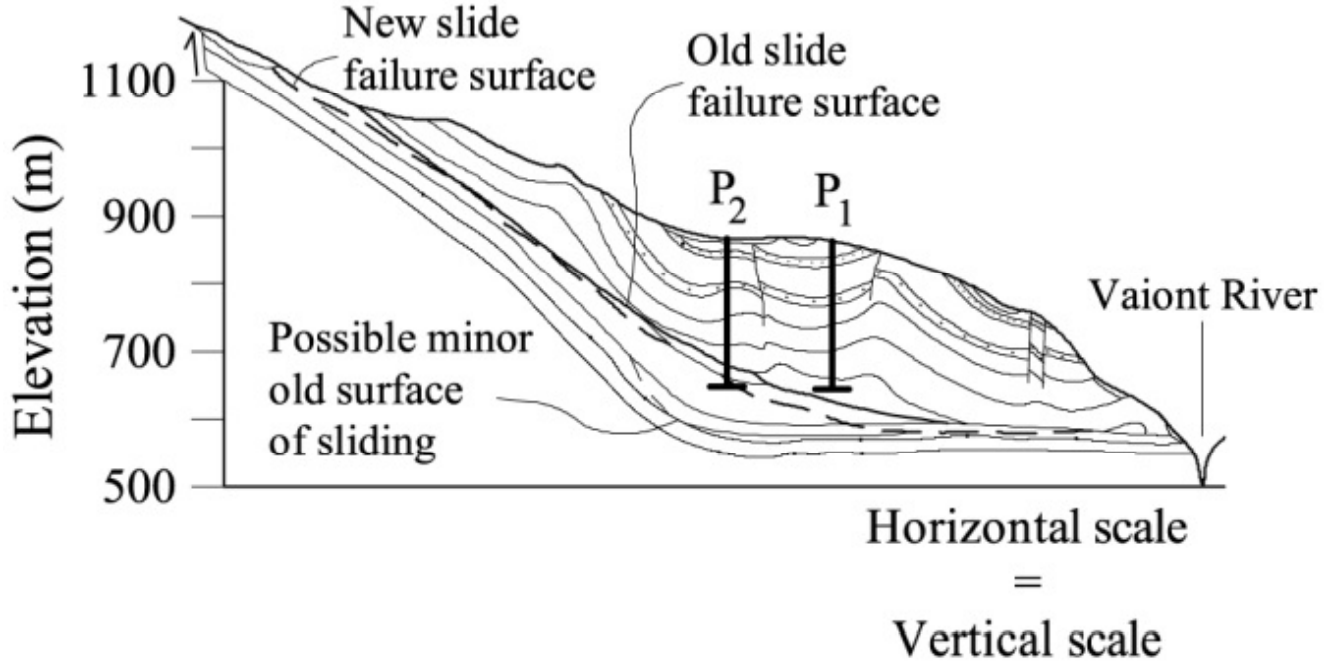

(After Hendron and Patton, 1985)

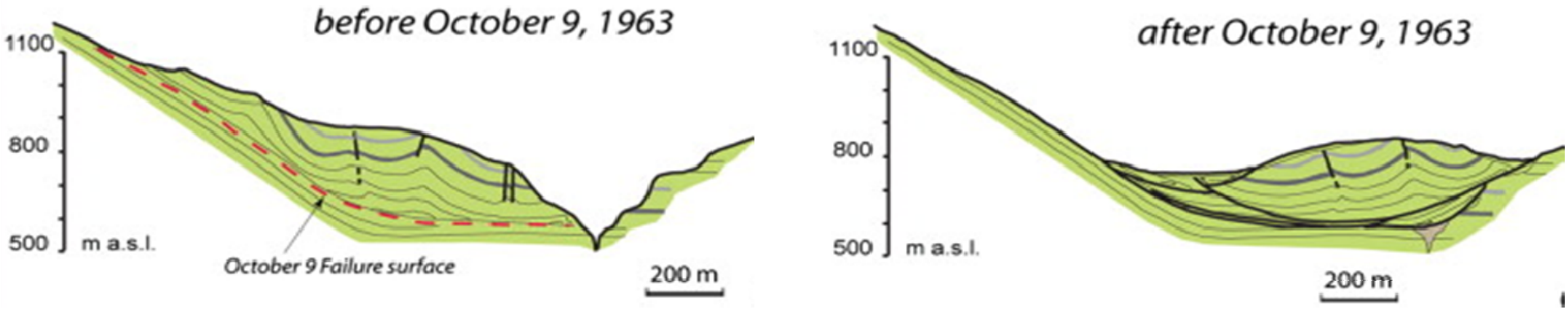

(from Del Ventisette, 2015; modified after Rossi and Semenza, 1965)

Kinematic constraints in compound slides

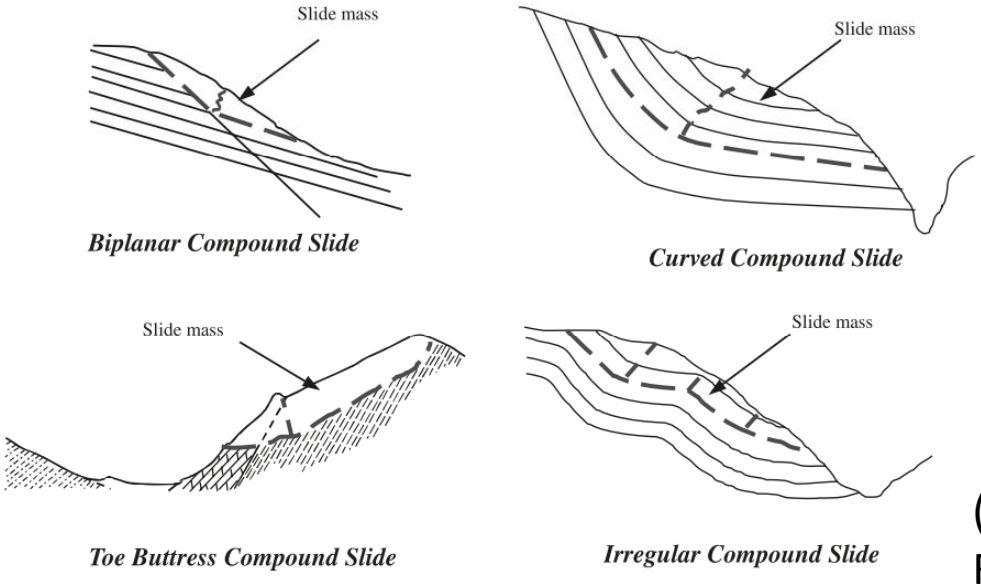

(Glastonbury and Fell, 2008).

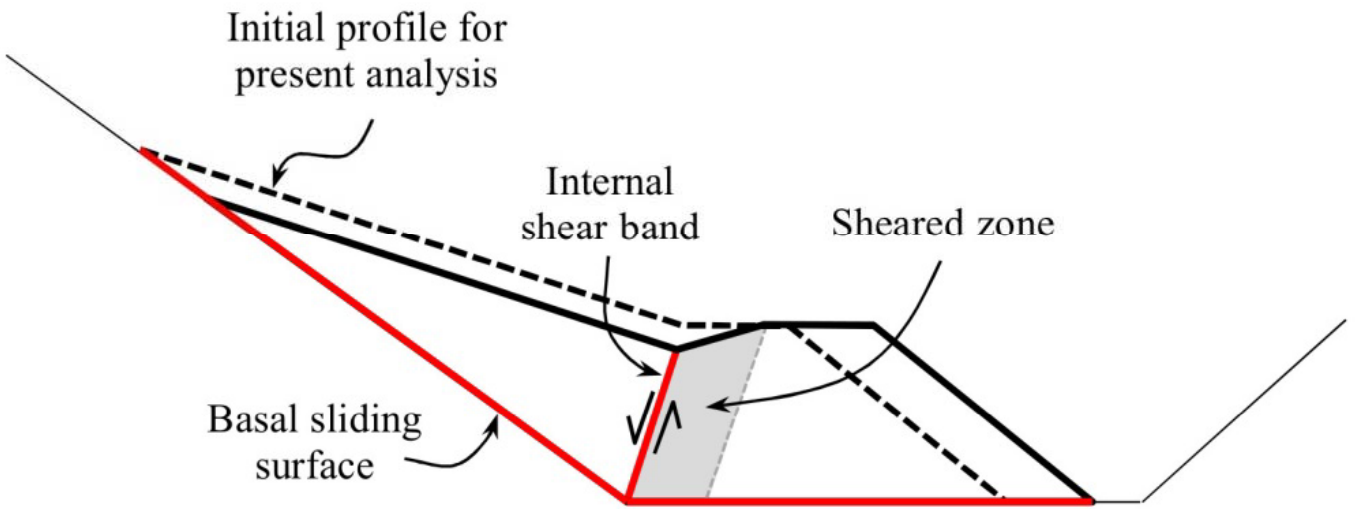

Geometry

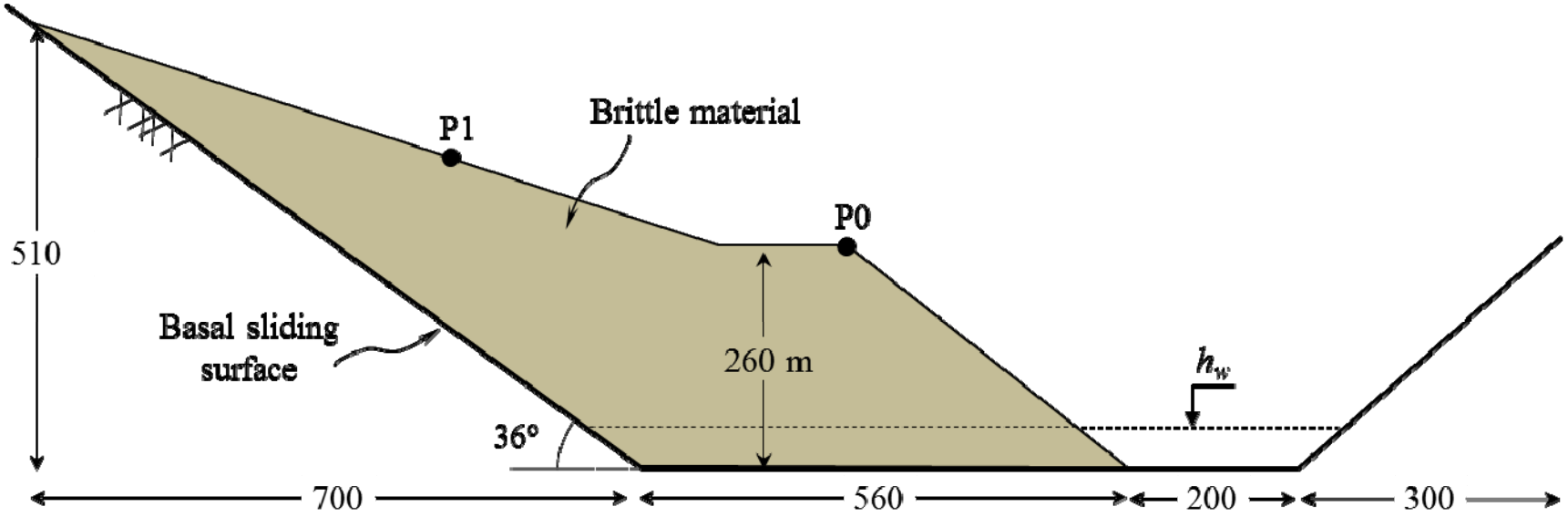
P1
Brittle material
P0
510
Basal sliding surface
260 m
h_w
36°
700
560
200
300

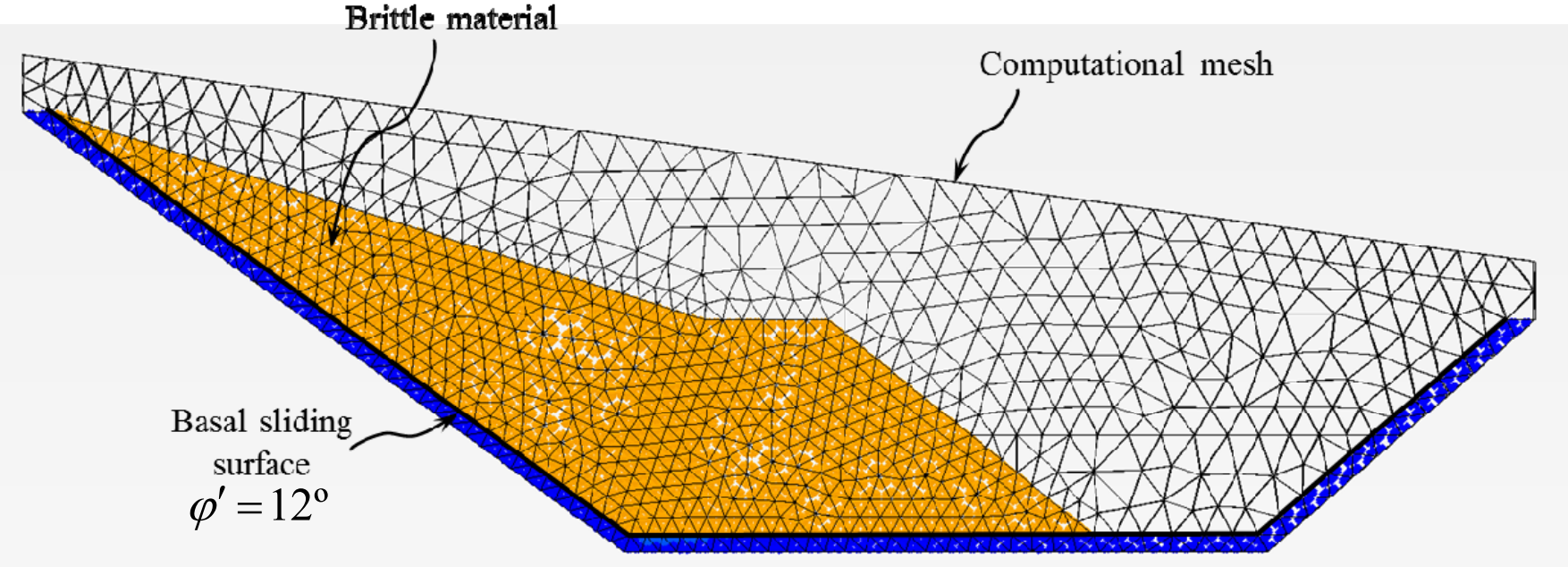
Brittle material
Computational mesh
Basal sliding surface
$\varphi' = 12°$

Initial state. Gravity effect

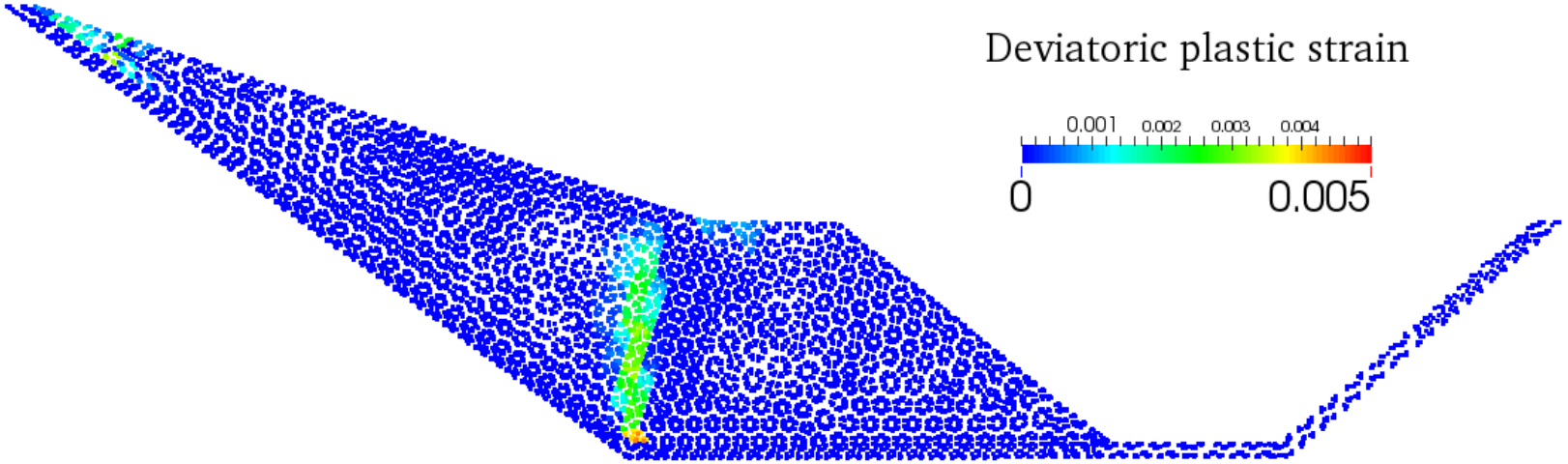

Internal degradation of rock mass
Increase water pressure

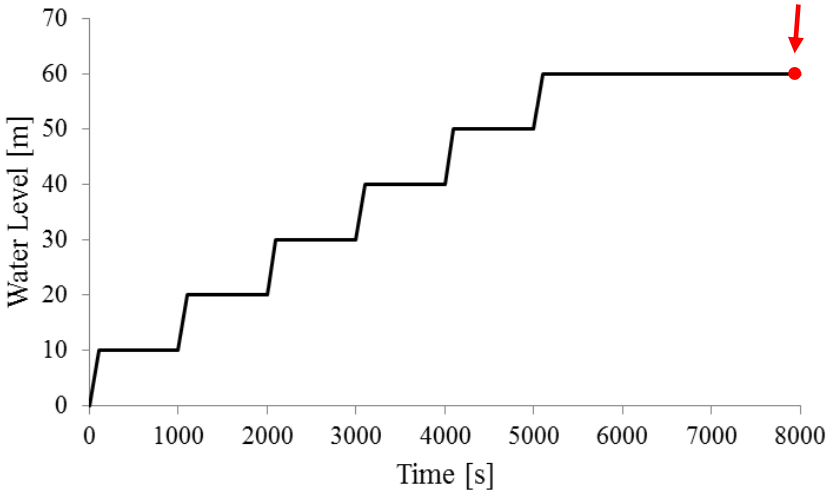

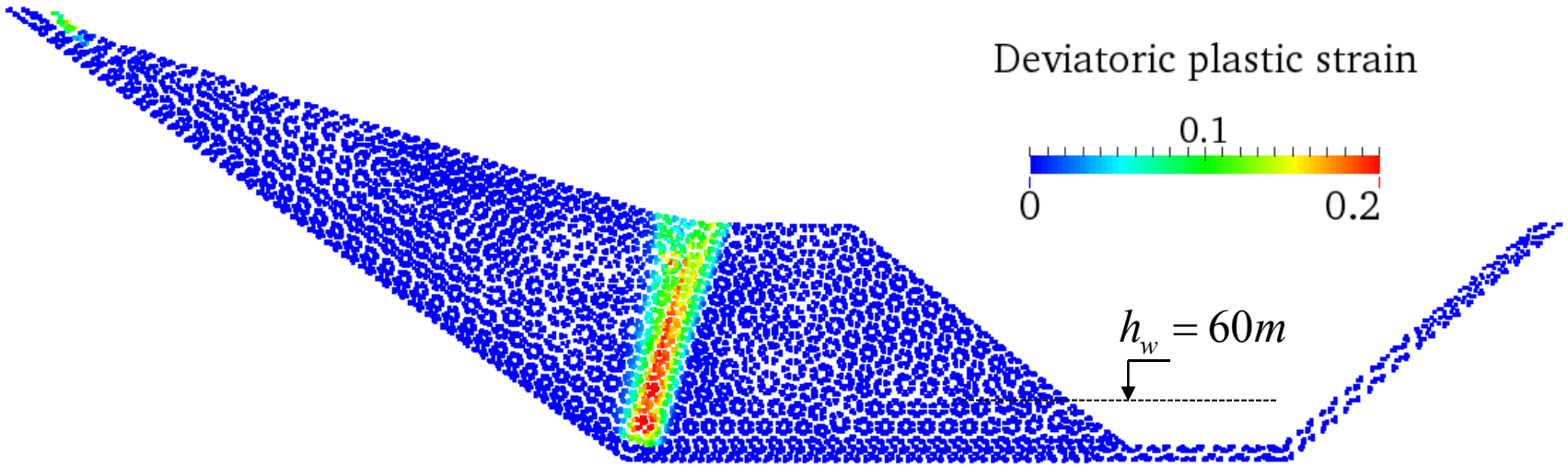

Slide kinematics during reservoir impounding

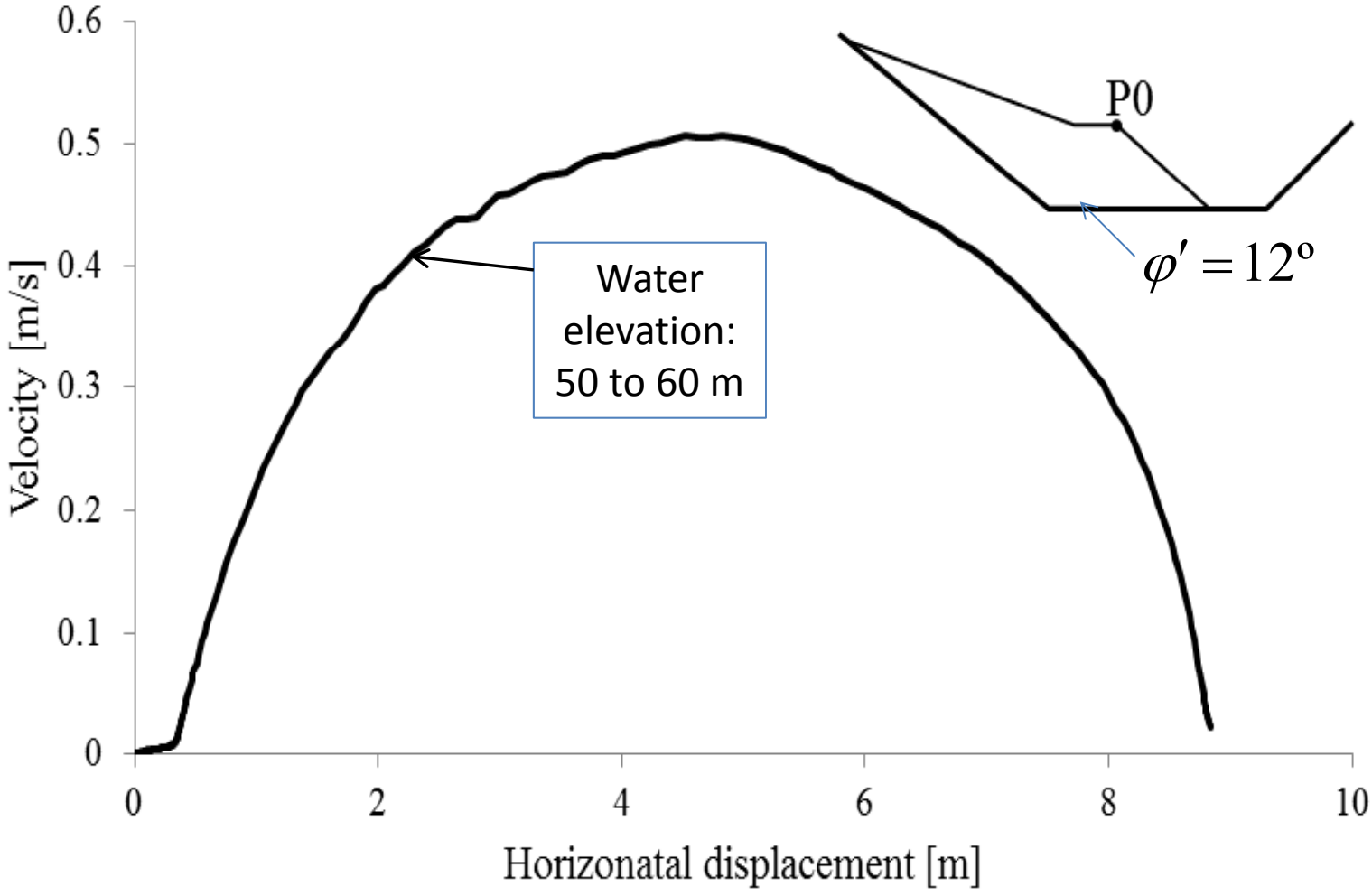

Reduction of basal surface friction angle

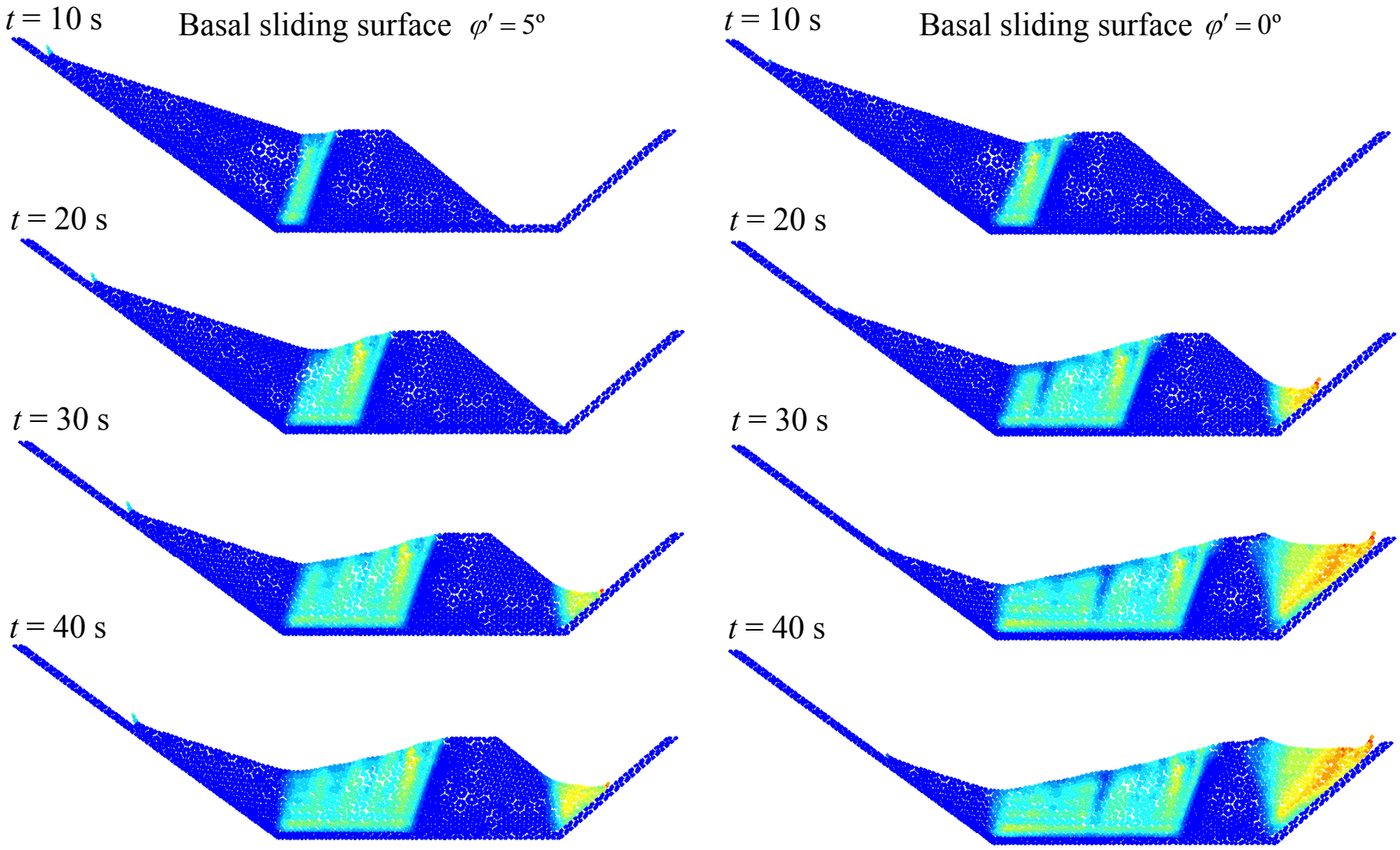

Kinematics of the reduction of basal surface friction angle

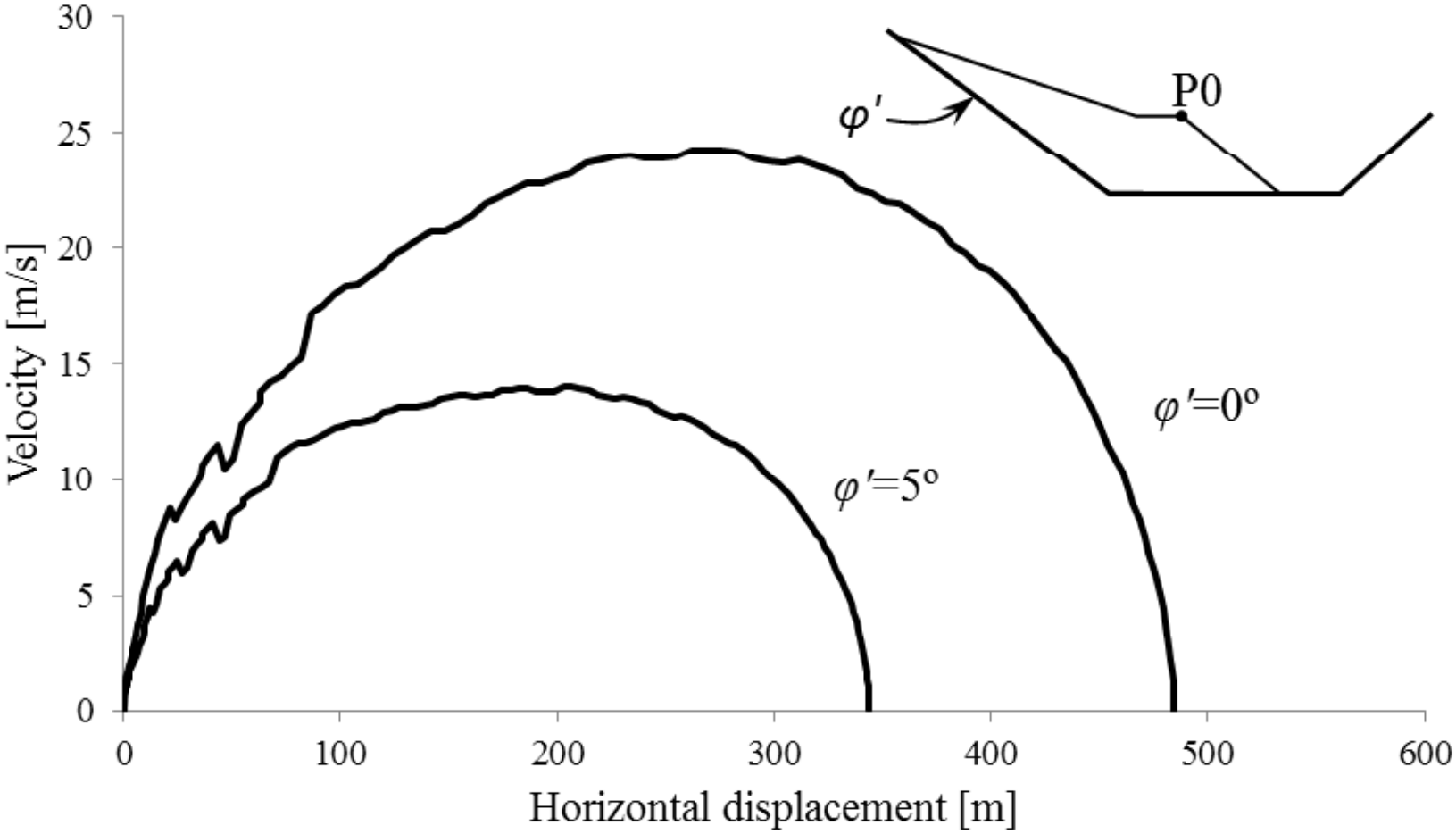


RAINFALL-INDUCED LANDSLIDES

Girona road embankments after heavy rainfall

Girona road embankments after heavy rainfall

Numerical model

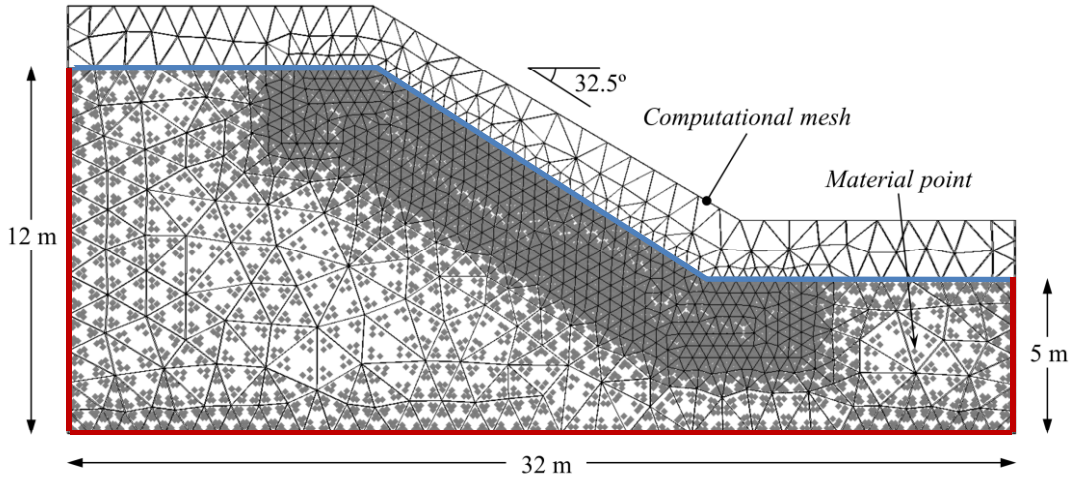

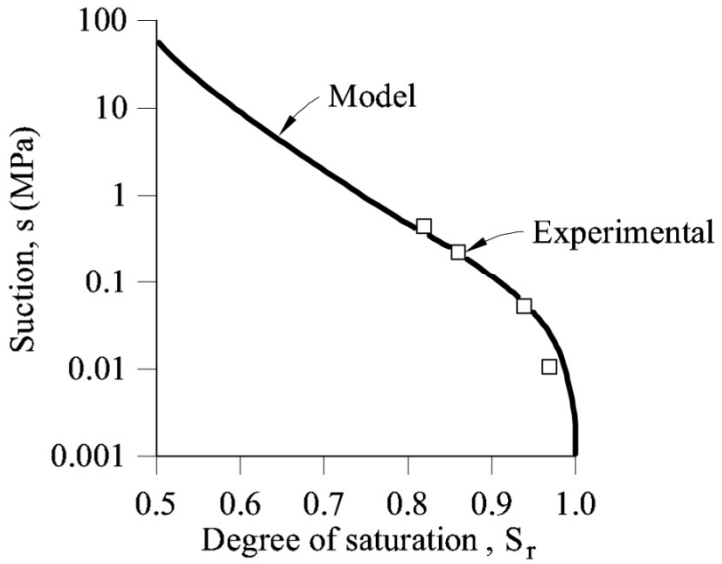

Element type	Tetrahedron	
Number of elements	3654	
Number of material points	7593	
Damping factor α	0.05	
Time step	$2 \cdot 10^{-4}$	S

Solid density ρ_s	2700	kg/m^3
Porosity n	0.35	
Poisson ratio ν	0.33	
Liquid density ρ_l	1000	kg/m^3
Gas density ρ_g	1	kg/m^3
Liquid bulk modulus K_l	100	MPa
Gas bulk modulus K_g	0.01	MPa
Liquid viscosity μ_l	10^{-3}	kg/m·s
Gas viscosity μ_g	10^{-6}	kg/m·s
Intrinsic permeability liquid k_l	10^{-10}	m^2
Intrinsic permeability gas k_g	10^{-11}	m^2

Young modulus E	10	MPa
Cohesion c'	1	kPa
Friction angle φ'	20	°
Δc_{max}	15	kPa
B	0.0007	
A	0.0001	

Embankment response

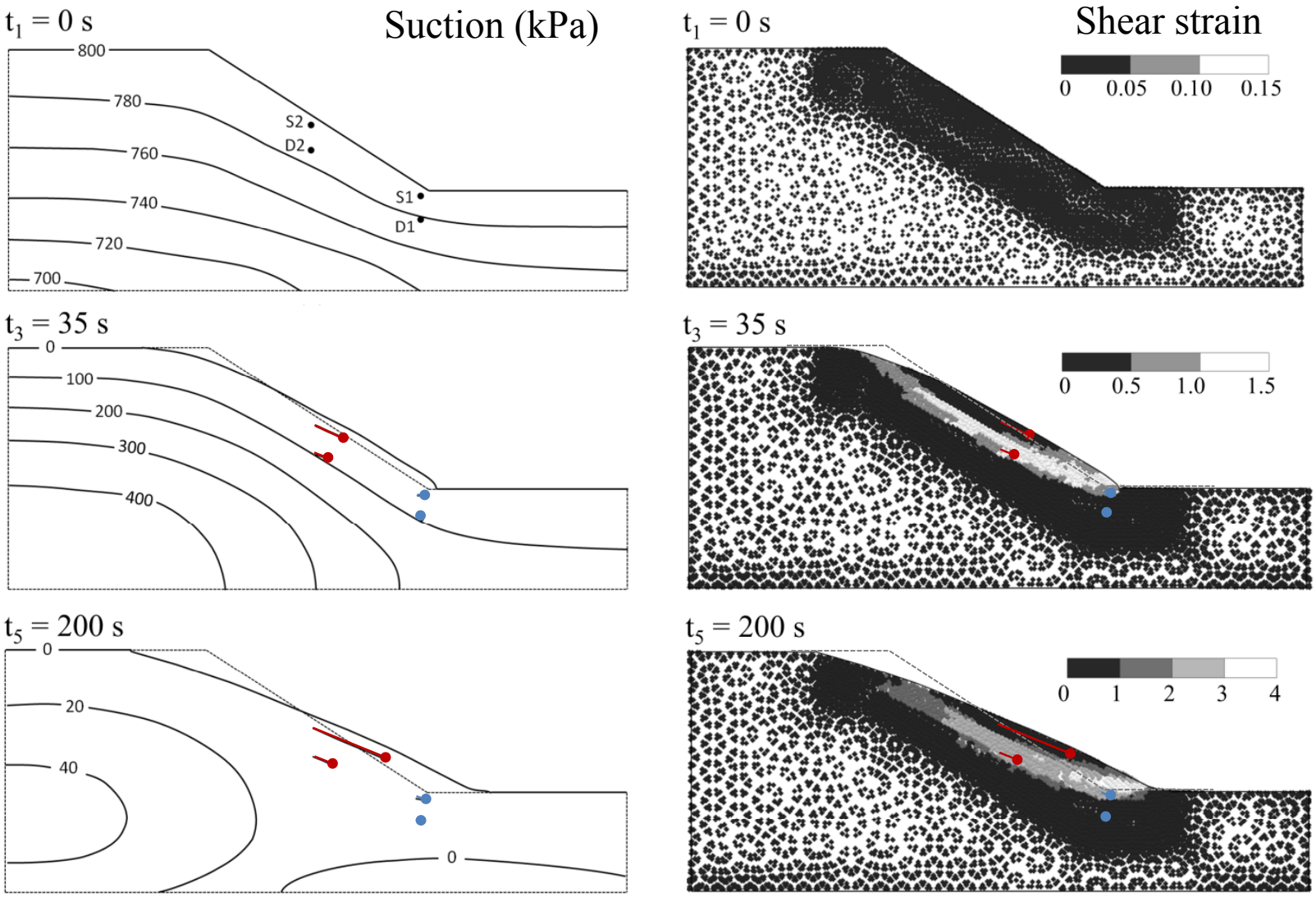

Dynamics of the motion

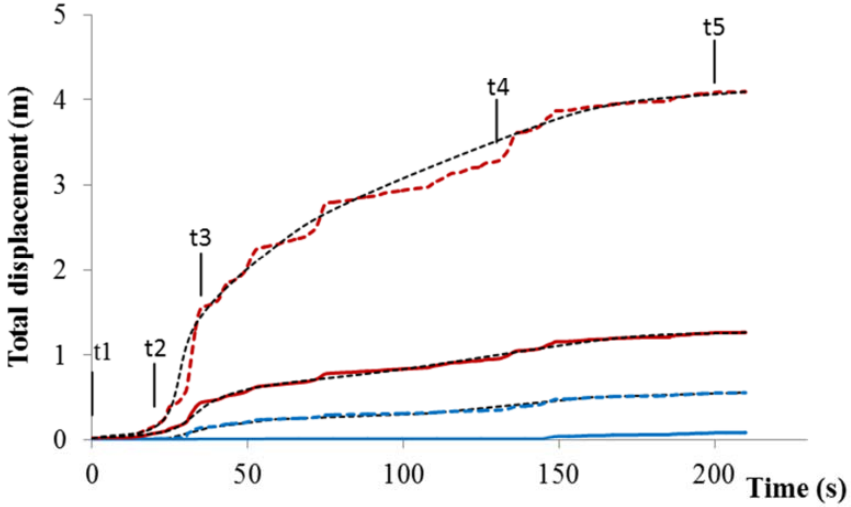

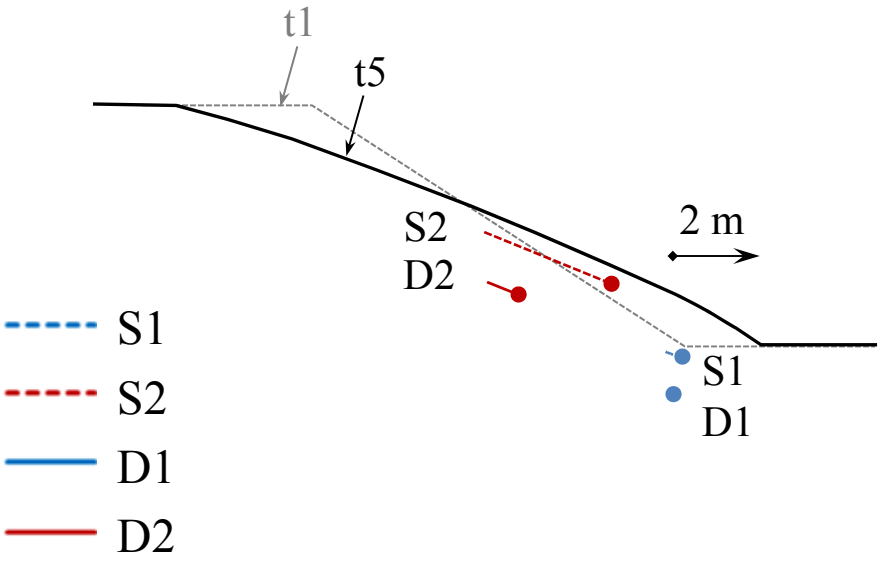

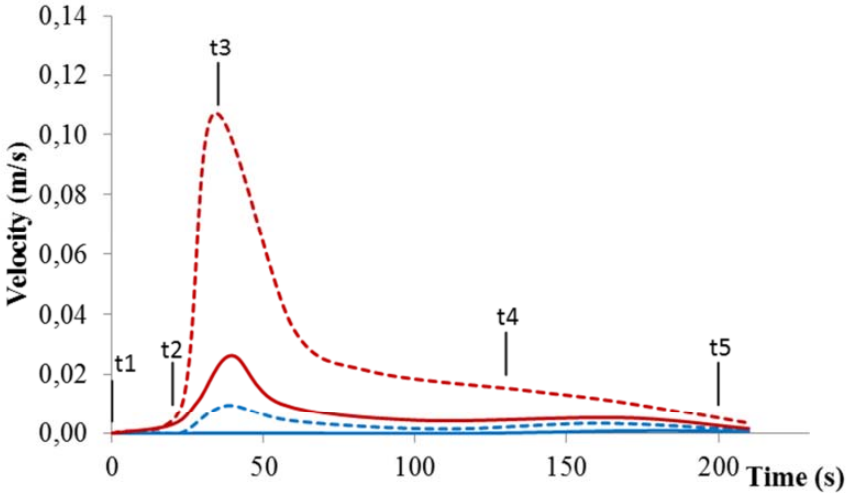

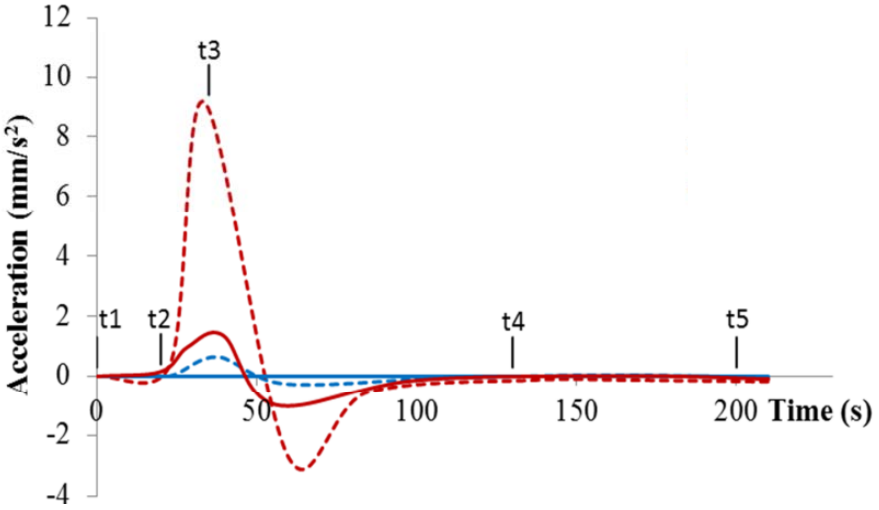

Oscillations

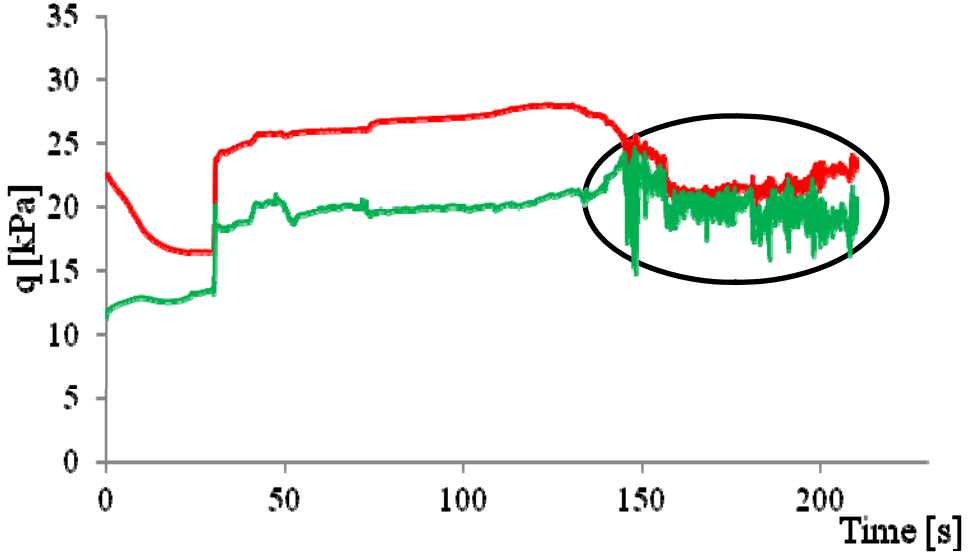

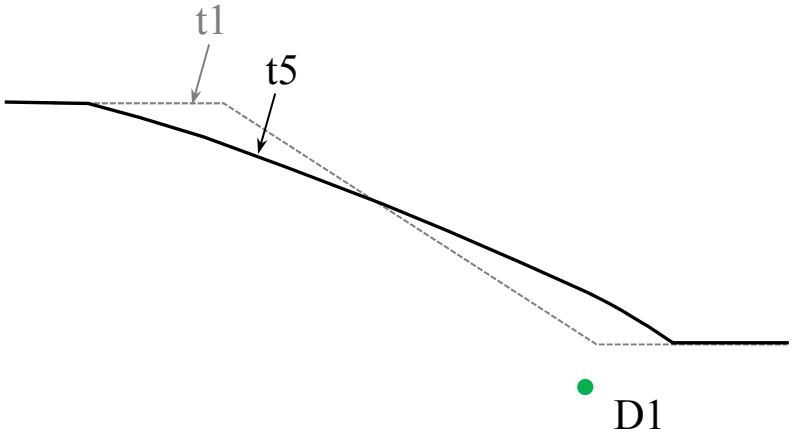

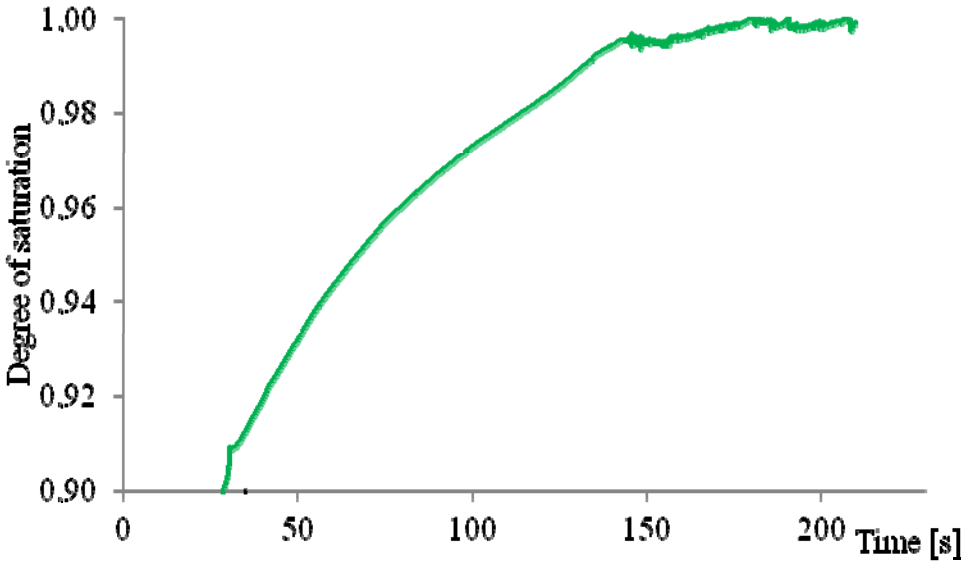

- Whenever there is an unbalanced force in a node, - MP crossing boundaries - some elastic waves are generated
- Strength softening
- Change in soil stiffness

Bulk stiffness of unsaturated soils

$$K_m = K_{sk} + \frac{1}{\frac{nS_l}{K_l} + \frac{n(1-S_l)}{K_g}}$$

Stiffness of the mixture increases abruptly when $S_l \to 1$

$$K_{sat} = K_{sk} + \frac{K_l}{n}$$

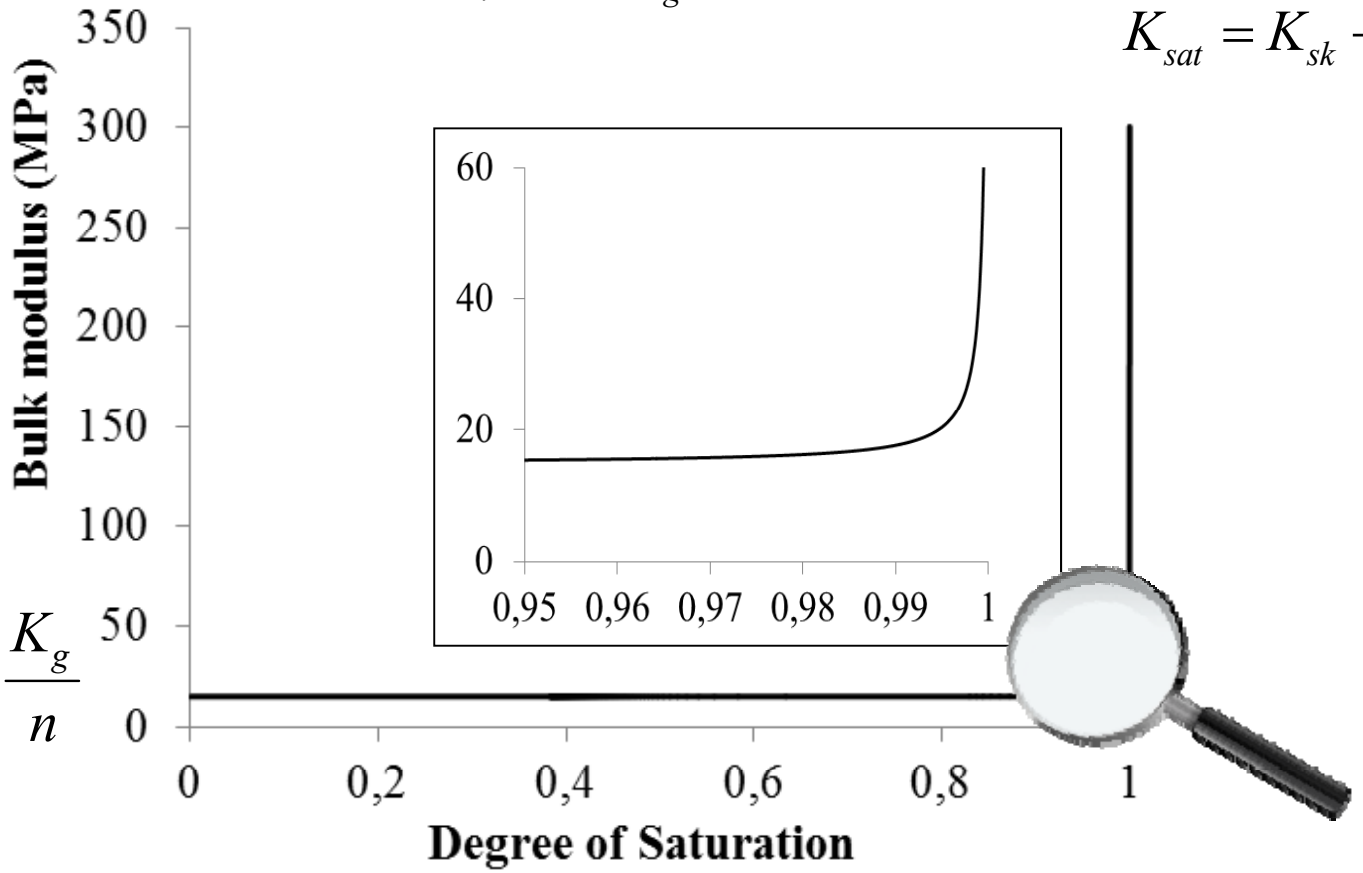

$$K_{dry} = K_{sk} + \frac{K_g}{n}$$

Conclusions

- STRONG POINTS OF MPM IN SLOPE STABILITY ANALYSIS
  - Incorporates FE methodologies
  - Well known constitutive equations
  - Dynamics+large deformations
  - Significant developments ahead
- SELBORNE EXPERIMENT
  - Consistent interpretation of progressive failure
  - Measured run-out reproduced
- COMPOUND LANDSLIDES
  - Number and location of internal shearing bands depend on geometry -specifically sliding surface geometry-
  - Support to thermal pressurization mechanisms in clayey shear bands
- RAINFALL-INDUCED SLIDING
  - Complex interaction between suction changes and instability. Complicated post-failure kinematics
  - The singularity of transition to full saturation

Acknowledgements

→ MPM Research Community

- Deltares, Delft
- University of Cambridge
- University of Hamburg
- UPC
- University of Padova
- TU Delft

Thank you for your attention!